The Pennsylvania State University

The Graduate School

College of Earth and Mineral Sciences

FORWARD MODELING OF COMPACTION AND FLUID FLOW

IN THE URSA REGION,

MISSISSIPPI CANYON AREA, GULF OF MEXICO

A Thesis in

Geosciences

by

Louanne Marie Christopher

Submitted in Partial Fulfillment
of the Requirements
for the Degree of

Master of Science

December 2006

I grant The Pennsylvania State University the nonexclusive right to use this work for the University's own purposes and to make single copies of the work available to the public on a not-for-profit basis if copies are not otherwise available.

Louanne Marie Christopher

The thesis of Louanne Marie Christopher was reviewed and approved* by the following:

Peter Flemings
Professor of Geosciences
Thesis Advisor

Andy Nyblade
Associate Professor of Geosciences

Kamini Singha
Associate Professor of Geosciences

Scott Barboza
Research Scientist
ExxonMobil Upstream Research Company

Kate Freeman
Professor of Geosciences
Associate Head of Graduate Programs and Research

*Signatures are on file in the Graduate School

ABSTRACT

Compaction models simulate the rapid deposition of low permeability sediments in the Ursa Region and account for the significant overpressure in the Ursa Region of the Gulf of Mexico. The models indicate that overpressure developed in the last 30 ky during the rapid deposition of low permeability clays and muds 1000 mbsf and above. The models also illustrate the flow focusing effect of the wedge geometry of the Ursa sediments and suggest that the sandy Blue Unit acts as a permeable conduit for lateral flow.

TABLE OF CONTENTS

LIST OF FIGURES

LIST OF TABLES

ACKNOWLEDGEMENTS

NOMENCLATURE / ABBREVIATIONS

Symbol	Description	Dimensions
a	matrix compressibility constant	$M^{-1}LT^2$
c_v	consolidation constant	$M^{-1}L^3T^{-1}$
$d\eta$	element length	L
dt	time step	T
dx	element length	L
dz	element length	L
g	gravitational acceleration	LT^{-2}
GR	gamma ray	-
h	height of sediment column	L
IODP	Integrated Ocean Drilling Program	-
K	diffusivity	$M^{-1}L^3T^{-1}$
k	permeability	L^2
k_0	initial permeability	L^2
km	kilometer	L
kPa	kilo Pascal	$ML^{-1}T^{-2}$
K_s	hydraulic conductivity	LT^{-1}
k_{xx}	average permeability	L^2
ky	thousands of years	T
kya	thousands of years ago	T
m	sedimentation rate	LT^{-1}
m	permeability exponent	-
m	meter	L
mD	millidarcy	L^2
m/yr	meters per year	LT^{-1}
mbsf	meters below sea floor	L
mm/yr	millimeter per year	LT^{-1}
MPa	mega pascal	$ML^{-1}T^{-2}$
MTCs	mass transport complexes	-
n	permeability exponent	-
OHMM	ohm-meter	ΩL
P	pore fluid pressure	$ML^{-1}T^{-2}$
$P*$	overpressure	$ML^{-1}T^{-2}$
P_d	dimensionless overpressure	-
P_h	hydrostatic pressure	$ML^{-1}T^{-2}$
psi	pounds per square inch	$ML^{-1}T^{-2}$
psi/ft	pounds per square inch per foot	$ML^{-2}T^{-2}$
q	flux	LT^{-1}
RES	resistivity	-

St	storativity	$M^{-1}LT^2$
t	time	T
tf	time factor	-
TVDSS	true vertical depth subsea	L
TWT	two way travel time	T
Z	depth below seafloor	L
β	bulk compressibility constant	$M^{-1}LT^2$
γ'	effective density constant	ML^{-3}
η	depth	L
$\lambda*$	overpressure ratio	-
μ	viscosity	$ML^{-1}T^{-1}$
ξ	dimensionless depth	-
ρ_b	bulk density	ML^{-3}
ρ_f	fluid density	ML^{-3}
ρ_s	solid density	ML^{-3}
σ_v	overburden stress	$ML^{-1}T^{-2}$
σ_v'	vertical effective stress	$ML^{-1}T^{-2}$
$\sigma_v'_h$	hydrostatic vertical effective stress	$ML^{-1}T^{-2}$
φ	porosity	-
φ_0	surface porosity	-
φ_η	element porosity	-

Chapter 1

Preface

This thesis contains two chapters and two appendices. Chapter 2 discusses one-dimensional modeling of sediment accumulation and consolidation in the upper 1000 mbsf of the Ursa Region in the Gulf of Mexico. A numerical model is implemented to gain insight to the development of overpressure. The model is compared to two analytical solutions to test its validity before applying the model to the Ursa Region. A brief description of the geology and structure of the Ursa Region is included and the derivation of constants and variables used in the simulation is also presented.

Chapter 3 describes the modeling results of 1- and 2-dimensional models of the Ursa Region using the numerical modeling application, Stellar™. This application makes use of seismic-based stratigraphic interpretations of the depositional history and illustrates how integrated modeling can provide additional validation of the depositional framework proposed by seismic stratigraphy. The modeling results predict the location and magnitude of overpressure development in the Ursa Region.

The appendices present a more detailed description of the derivation and implementation of the finite-difference solution and matrix inversion of the diffusion equation used in the numerical model. Additionally, the Matlab® code used in the numerical model is presented as a reference.

Chapter 2

1-D Compaction flow modeling of Ursa Region

2.1 Abstract

Results from one-dimensional compaction models underpredict the estimated overpressure from the Integrated Ocean Drilling Program (IODP) Expedition 308 drill sites in the Ursa Region. The numerical models are used to illustrate how the regional overpressure is tied to the initial conditions of deposition, and more specifically, to porosity and permeability profiles of the sediments deposited. The forward models are implemented using a finite-difference approximation to the diffusion equation. They are tested by comparison with two analytical models, a diffusion solution by Turcotte and Schubert (2002) and the Gibson (1958) sedimentation model. The models are then populated with parameters to simulate the conditions in the Ursa Region.

2.2 Introduction

Compaction modeling focuses on fluid behavior as sediments compact and has been studied extensively by civil and structural engineers, hydrogeologists, and industry geologists. Gibson (1958) provided an analytical solution that coupled sedimentation and flow in one dimension. Subsequent authors have explored numerical models to extend this work to two and three dimensions (Bredehoeft and Hanshaw, 1968; Bethke, 1985; Bethke and Corbet, 1988; Palciauskas and Domenico, 1989; Audet and Fowler, 1992; Fowler and Yang, 1998; Gordon and Flemings, 1998; Chen et al., 2002). Additionally, models seeking to quantify the effects of sediment loading versus alternative pressure generation sources, such as thermal effects and mineral diagenesis have indicated that sediment loading is the dominant source of overpressure where sedimentation is rapid (Bethke, 1986; Harrison and Summa, 1991; Luo and Vasseur, 1992; Gordon and Flemings, 1998).

The petroleum industry uses compaction models to predict pressure and reduce drilling risks. This study uses a numerical model developed in Matlab® (the Matlab® model) as a tool to characterize an overpressured system and documents the utility of the tool for enhancing the geological understanding obtained from regional seismic and boreholes drilled in the Ursa Region by the Integrated Ocean Drilling Program (IODP) Expedition 308. The study focuses on the depth of onset of pressure in excess of hydrostatic pressure or overpressure, and attempts to identify the source and timing of overpressure generation in the Ursa region.

2.3 Compaction Model

The compaction model describes the behavior of pore fluids in a saturated column of sediment (Figure 2-1). Under hydrostatic conditions, fluid pressure, P, follows a pressure gradient with depth of approximately 9.5 kPa/m (0.45 psi/ft). Pore pressures can lie above hydrostatic pressure and this is termed overpressure, $P*$ (Figure 2-2). The vertical effective stress, σ_v', is the difference between the overburden stress and the fluid pressure in the pores.

$$\sigma_v' = \sigma_v - P. \tag{2.1}$$

Hydrostatic effective stress, $\sigma_v'{}_h$, is the difference between the overburden stress and hydrostatic pressure, P_h,

$$\sigma_v'{}_h = \sigma_v - P_h. \tag{2.2}$$

An overpressure ratio, $\lambda*$, gives the ratio of overpressure to hydrostatic effective stress and is a measure of how closely the overpressure approches the overburden stress.

$$\lambda^* = \frac{P - P_h}{\sigma_v - P_h}. \tag{2.3}$$

$\lambda*$ varies from 0 (when $P = P_h$) to 1 (when $P = \sigma_v$). Low values of $\lambda*$ record completely drained systems, while high values indicate an undrained system. Values very close to 1 indicate that the fluid pressure is very close to the overburden stress and imply that the pore fluids are bearing all the load. An overpressure ratio of 0 indicates that there is no overpressure, or that the fluid pressure is hydrostatic.

Figure 2-1
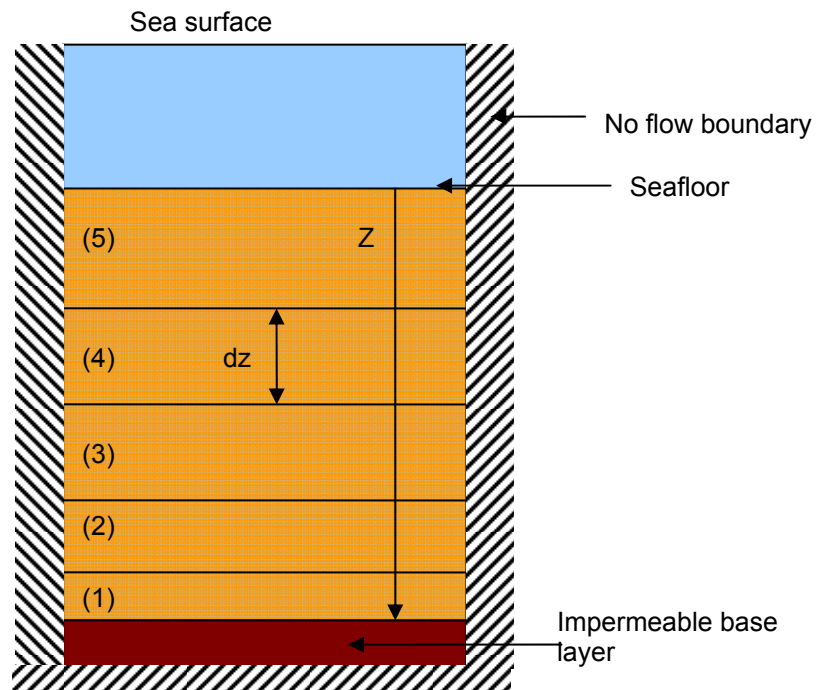
Figure 2-1: A saturated sediment column is modeled with 5 layers above an impervious base layer. Lateral no-flow boundaries restrict flow to the vertical direction. Sedimentation drives compaction, and overpressure may develop if pore fluids are unable to drain. Depth below the seafloor (Z) is measured to the top of the impermeable layer and layer thickness is tracked as the column compacts.

Figure 2-2
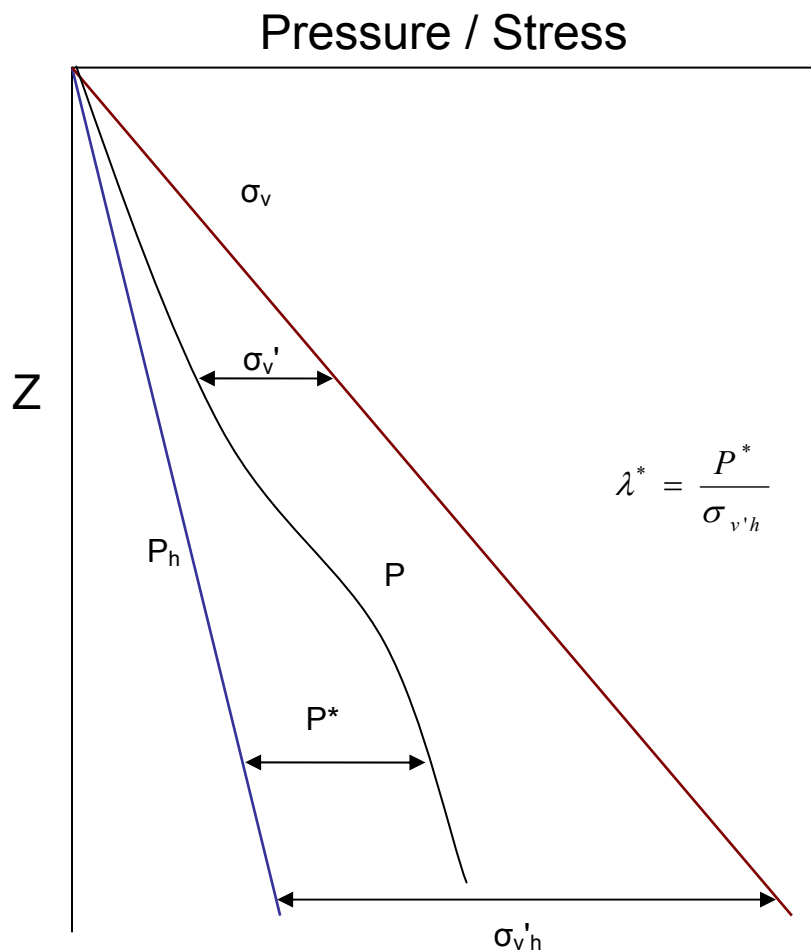
Figure 2-2: A pressure-depth plot shows how fluid pressure, P, may vary between hydrostatic pressure, P_h, and overburden stress, σ_v. Fluid pressure is discussed in terms of overpressure, P^*, or pressure in excess of hydrostatic. The load that the rock matrix bears is called the effective stress, σ_v'. Effective stress divided by the hydrostatic effective stress ($\sigma_v'_h$) gives the overpressure ratio, λ^*. Depth, Z, is measured from the sea floor.

The compaction model used here is based on the form of the diffusion equation as derived by Gordon and Flemings (1998):

$$\frac{DP}{Dt} = \frac{k(1-\phi_\eta)^2}{\mu St \rho_f g} \frac{D^2 P^*}{D\eta^2} + \beta \frac{\phi_\eta}{St(1-\phi_\eta)} \frac{D\sigma_v}{Dt}.$$

(2.4)

The first term on the right hand side models pressure diffusion. The controlling parameters for pressure diffusion are permeability *(k)*, fluid viscosity *(μ)*, and porosity *(φ$_\eta$)*. *St* is a storage coefficient dependent on porosity and matrix compressibility *(β)*. *g* is acceleration due to gravity, and ρ_f is fluid density.

$$St = \frac{\phi_\eta \beta}{1-\phi_\eta}.$$

(2.5)

The second term on the right hand side of Equation 2.4 is a source term due to sediment loading. This term is primarily controlled by the sedimentation rate. Additional source terms for thermal effects and diagenesis are ignored here.

The diffusive term and source terms are uncoupled and solved separately at each time step. The diffusive term is rewritten using a finite-difference approximation. The subscripts *x, x-1* and *x+1* indicate cell number and subscripts *x+1, x* or *x, x-1* denotes that an average (harmonic) is used to represent the boundary between 2 adjacent cells. (Asterisk denoting overpressure is omitted for simplicity in equation below).

$$\frac{dP_x}{dt} = \left[\frac{K_{x+1,x}(P_{x+1}^{t+1} - P_x^{t+1}) - K_{x,x-1}(P_x^{t+1} - P_{x-1}^{t+1})}{(dx)^2} \right]$$

(2.6)

$$where\ K_{x+1,x} = \frac{k_{x+1,x}}{\mu} \frac{(1-\phi_{x+1,x})^2}{St_{x+1,x}\rho_f g}.$$

Equation 2.6 is solved by matrix inversion. All calculations and results are presented as at the grid cell centers. Details of the finite-difference implementation are presented in Appendix A.

Initial porosity, φ_0, grain density, ρ_s, fluid density, ρ_f, viscosity, μ, and matrix compressibility, β, were assumed constant throughout the simulation (Table 2-1).

Table 2-1

Table 2-1: Simulation Constants

Parameter	Symbol	Value (units)
Fluid density	ρ_f	1024 (kg/m^3)
Grain Density	ρ_s	2720 (kg/m^3)
Gravitational acceleration	g	9.81 (m/s^2)
Reference porosity	φ_0	0.61 (m^3/m^3)
Matrix compressibility	β	1.48 x 10^{-7} (Pa^{-1})
Viscosity	μ	1 (cp)

2.4 Matlab® model Validation

The numerical solution was validated using two analytical 1-D solutions: Turcotte and Schubert's (2002) diffusion of heat through a finite column and Gibson's (1958) sedimentation model.

2.4.1 Diffusion within a sediment column (Turcotte and Schubert, 2002)

Turcotte and Schubert's analytical solution describes the diffusion of heat due to an imposed temperature change at one boundary through a sediment column of finite thickness (Figure 2-3). Their solution is equally applicable to the diffusion of overpressure, since the base equation (shown below) is mathematically equivalent.

$$\frac{\partial P^*}{\partial t} = K \frac{\partial^2 P^*}{\partial x^2}.$$

(2.7)

At the base of a sediment column, a constant overpressure is assumed, and overpressure diffuses to the surface. Mathematically, these boundary conditions are expressed as:

(i) $P^* = 0$ at all x, for $t = 0$,

(ii) $P^* = P^*_2$ at $x = Z$ for $t > 0^+$, and

(iii) $P^* = 0$ at $x = 0$ for $t > 0^+$.

Turcotte and Schubert's (2002) solution is expressed as:

$$P_x^t = P_x^{0-} + \left(P_Z^{0+} - P_x^{0-}\right)\left[\frac{x}{Z} + \frac{2}{\pi}\sum_{n=1}^{\infty}\frac{1}{n}\exp\left(-\frac{Kn^2\pi^2 t}{Z^2}\right)\sin\left(\frac{n\pi x}{Z}\right)\right].$$

(2.8)

(The asterisk is omitted for simplicity.) The subscript, x, indicates location. Diffusivity, K, is calculated as follows:

$$K = \frac{k}{\mu}\frac{(1-\phi)^2}{St\rho_f g}.$$

(2.9)

Figure 2-3
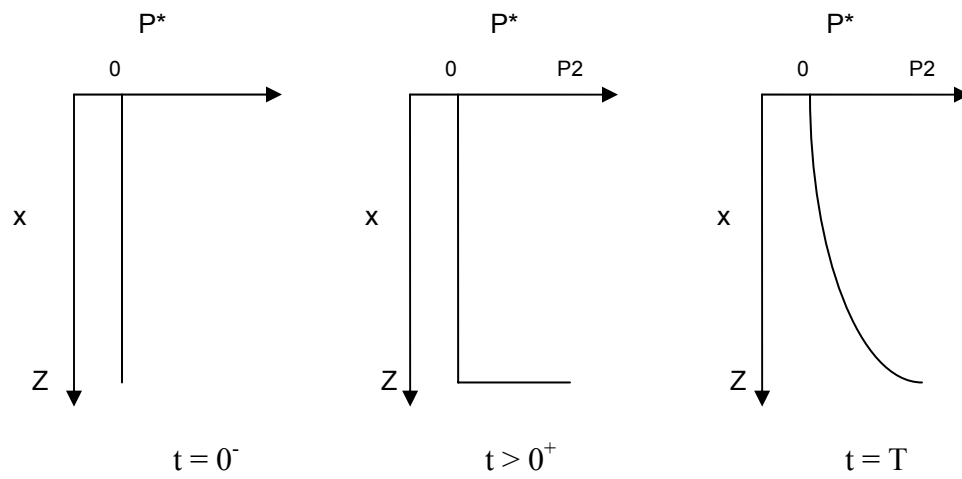
Figure 2-3: A column that is initially at zero overpressure experiences an instantaneous and constant increase in overpressure at the base. The base overpressure (P2) diffuses through the column over time. The overpressure profile at time, T, can be calculated using an analytical solution (Adapted from Turcotte and Schubert, 2002).

Note that the analytical solution requires a constant diffusivity (K). The model assumes that strain is minor.

The Matlab® model is tested using 3 different values of diffusivity, which are calculated by varying permeability while values of porosity, viscosity and matrix compressibility from Table 2-1 are used. Initially, overpressure is zero throughout the column. At t = 0, an overpressure of 6 MPa is prescribed at the base and held constant. Results are obtained after a period of 80 ky.

The numerical solution in Matlab® slightly overpredicts the analytical solution. Percentage error in the Matlab® model is calculated using the difference between the analytical solution and the numerical model, relative to the analytical solution.

The average error between the Matlab® model and analytical solution is less than 15 %. The Matlab® model performed best with low permeability runs, where the average error was less than 7 % of the analytical solution. The percentage error was greatest at points farthest from the prescribed overpressure boundary at the base. Figure 2-4 shows comparison overpressure profiles after a time of 80 ky has elapsed with the different diffusivities indicated.

Figure 2-4
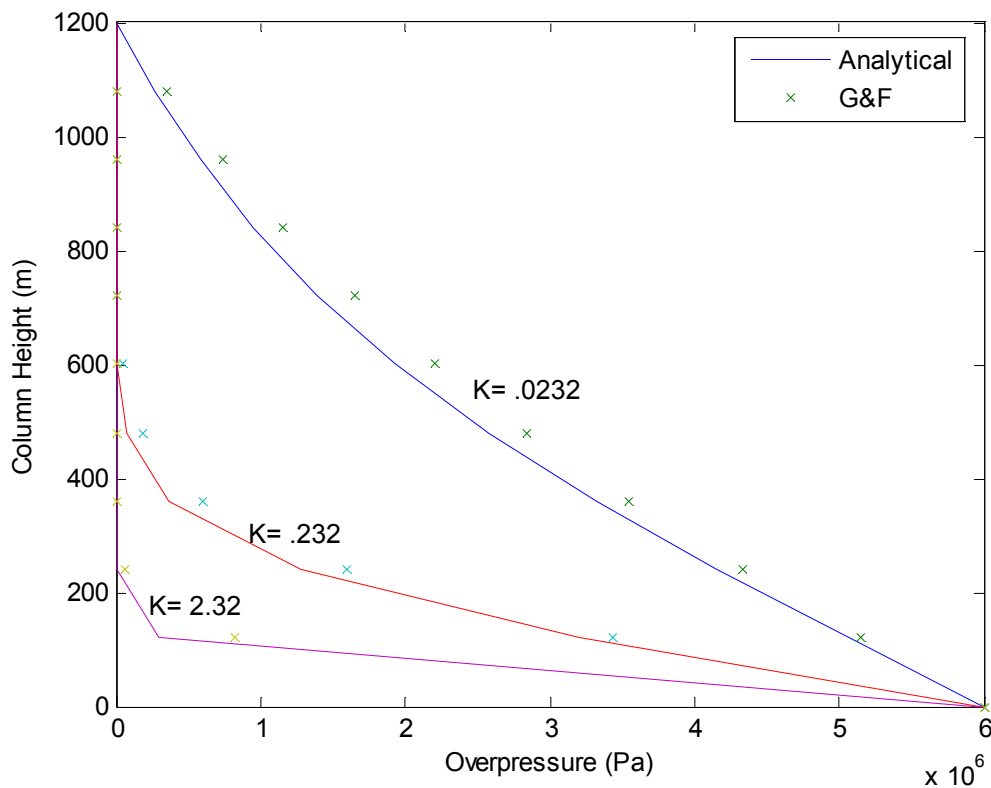
Figure 2-4: Comparison of analytical solution with a Matlab® model of the diffusion of a 6 MPa overpressure imposed and held constant at the base of a sediment column that has no overpressure initially. Profile is shown for results after 80 ky, with 1200 m of accumulated sediment. Diffusivity values for different runs are indicated on the graph. Model inputs are described in Section 2.4.1.

2.4.2 Gibson (1958) sedimentation model

The Gibson sedimentation model tracks the pressure of fluid within a saturated column of low permeability sediment that receives additional sedimentation at the surface (Figure 2-1). The Gibson equation solves:

$$\frac{\partial P*}{\partial t} = c_v \frac{\partial^2 P*}{\partial x^2} - \gamma' \frac{dh}{dt}.$$ (2.10)

x is depth within the sediment column and h is the total height of the sediment column at any time. Boundary conditions for this model are:

(i) $P* = 0$ at $x = 0$, and

(ii) $dP*/dx = 0$ at $x = Z$.

Gibson's analytical solution for these boundary conditions is:

$$P* = \rho_b mt - \rho_b \sqrt{\frac{1}{\pi c_v t}} \exp\left(\frac{-x^2}{4c_v t}\right) \int_0^\infty \xi \tanh\left(\frac{m\xi}{2c_v}\right) \cosh\left(\frac{x\xi}{2c_v t}\right) \exp\left(\frac{-\xi^2}{4c_v t}\right) d\xi$$ (2.11)

$$\text{where } \xi = \frac{x}{h(t)} \text{ and } 0 < x < Z.$$

ρ_b is bulk density, m is sedimentation rate, and t is time. Gibson's coefficients, c_v and γ', are modified below to match the Gordon and Flemings' formulation. Gibson assumes that diffusivity (c_v) is constant.

$$c_v = \frac{k(1-\phi_0)^2}{\mu St \rho g}.$$

$$\gamma' = \frac{\beta \phi_0}{St(1-\phi_0)}.$$ (2.12)

Results are plotted in units of dimensionless overpressure and dimensionless depth for several different 'time factors'. Dimensionless overpressure, P_d, is the ratio of overpressure to the hydrostatic effective stress. This is equivalent to $\lambda*$.

$$P_d = \frac{P*}{\gamma' h}.$$ (2.13)

Dimensionless depth, D_d, is a ratio of column height, x, to final column height, Z.

$$D_d = \frac{x}{Z}.$$ (2.14)

The time factor, tf, is a dimensionless ratio of sedimentation rate (m) to system compressibility (c_v):

$$tf = \frac{m^2 t}{c_v}.$$ (2.15)

A larger time factor represents a sedimentation rate that exceeds the ability of the sediments to drain. Large time factors occur with rapid sedimentation or low permeability sediments.

For all time factors, the Matlab® model gives slightly larger overpressures than the Gibson formulation (Figure 2-5). Percentage error in the Matlab® model is calculated using the difference between Gibson and numerical model, relative to the Gibson result. The percentage error is calculated at specific depth points, and an average error as well as the maximum error is recorded.

The percentage error varies from less than 2 % to 48 % difference between the two models (Table 2-2). The largest errors were recorded near the base of the sediment column. When very small time factors ($tf < 0.1$) are modeled, simulation results for both

models are hydrostatic. Generally, closest agreement between the models occurs with

large time factors.

Table 2-2: Percentage error between Matlab® model and Gibson solution for different time factors. Error is calculated relative to the Gibson result.

Time factor	Average Error	Max. Error
0.025	4 %	23 %
0.25	44 %	48 %
2.5	21 %	22 %
25	2 %	4 %
250	1.6 %	3 %

Figure 2-5
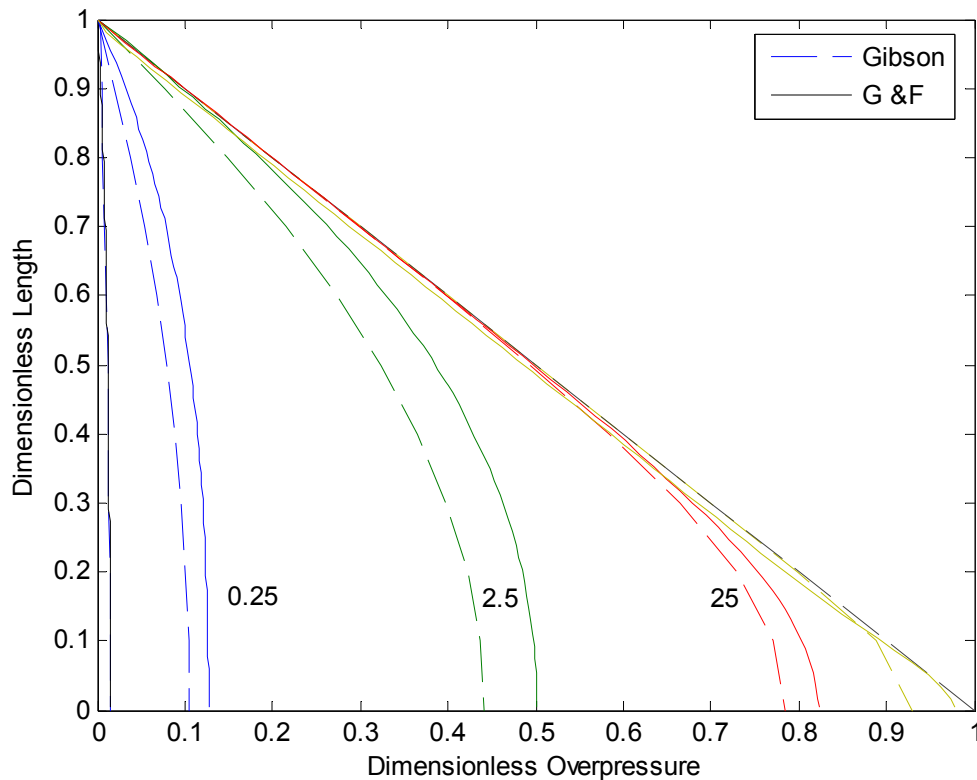
Figure 2-5: Comparison of Gibson solution and Matlab® model show disparity on a dimensionless overpressure – dimensionless depth plot. Dimensionless overpressure is overpressure divided by lithostatic stress and dimensionless length is depth at any point divided by total column depth. Labels show the time factor, a ratio of sedimentation rate to system compressibility. Model inputs are described in Section 2.4.2.

2.5 Ursa Region Geology

The Ursa Region is located 200 km southeast of New Orleans on the continental slope of the Gulf of Mexico (Figure 2-6). It is a salt-withdrawal mini-basin in 800-1400 meters of water, with sediments derived from late Pleistocene deposition by the Mississippi River system. The seafloor dips to the southeast and a zone of slope failures is present to the east of the Mars-Ursa region (Figure 2-6). This study focuses on the shallow sections of Ursa Region above 1000 meters below seafloor (mbsf), over an area of approximately 900 square kilometers (Figure 2-7). This depth interval includes the thick sandy package, called the Blue Unit, and the sediments that overlie it (Figure 2-8). A summary of Ursa basin geology follows but the basin is well described in the following papers: Eaton (1999); Winker and Booth (2000); Winker and Shipp (2002); Expedition 308 scientists (2005); Sawyer et al. (in press). We adopt their naming convention for major sediment packages.

The Blue Unit is a unit of interbedded sand and mud which extends over 150 km (Figure 2-9). It is thickest in the western part of the study area and thins to the east. The base of the Blue Unit is flat while the top reflects post-depositional erosion. It is incised by two channel levee systems, the Ursa Canyon and the Southwest Pass Canyon. The Southwest Pass Canyon lies to the west of the Ursa Canyon and is younger. These systems have mud rich levees with sandy channel fill (Figure 2-10). They cut through the Blue Unit in an approximately north-south orientation.

Above the channel levee systems, several mass transport complexes (MTCs) are observed in seismic data. These mass transport complexes are identified in this study as

Failure 1 and Failure 2 and are highlighted on the interpreted seismic cross-section. These are capped by 50-100 meters of hemipelagic drape.

The Ursa Region system is of particular interest as an overpressured system, which has been extensively mapped and drilled. Overpressure at Ursa is attributed to rapid deposition of the shallow sediments during the late Pleistocene. Average sedimentation rate for Ursa was calculated to be 0.015 m/yr using age data from three surfaces at Ursa (Sawyer et al, in press). The presence of the foraminifera *Globorotalia flexuosa* at the Base Blue puts this datum at approximately 70 thousand years ago (kya) (Sawyer et al, in press; Winker and Booth, 2000). Seismic surface S60 is dated to be approximately 60 kya, while surface S30 is dated at 25 kya.

Overpressure is present within 50 mbsf and approaches 70 % of the hydrostatic effective stress (Expedition 308 Scientists, 2005). This overpressure distribution has made drilling through the Blue Unit difficult and costly (Eaton, 1999). This study seeks to further characterize the overpressure field of the Ursa Basin by multi-dimensional modeling to identify the extent and impact of connectivity of the Blue Unit sands on overpressure, and identify potential bypass zones for safer drilling.

Figure 2-6
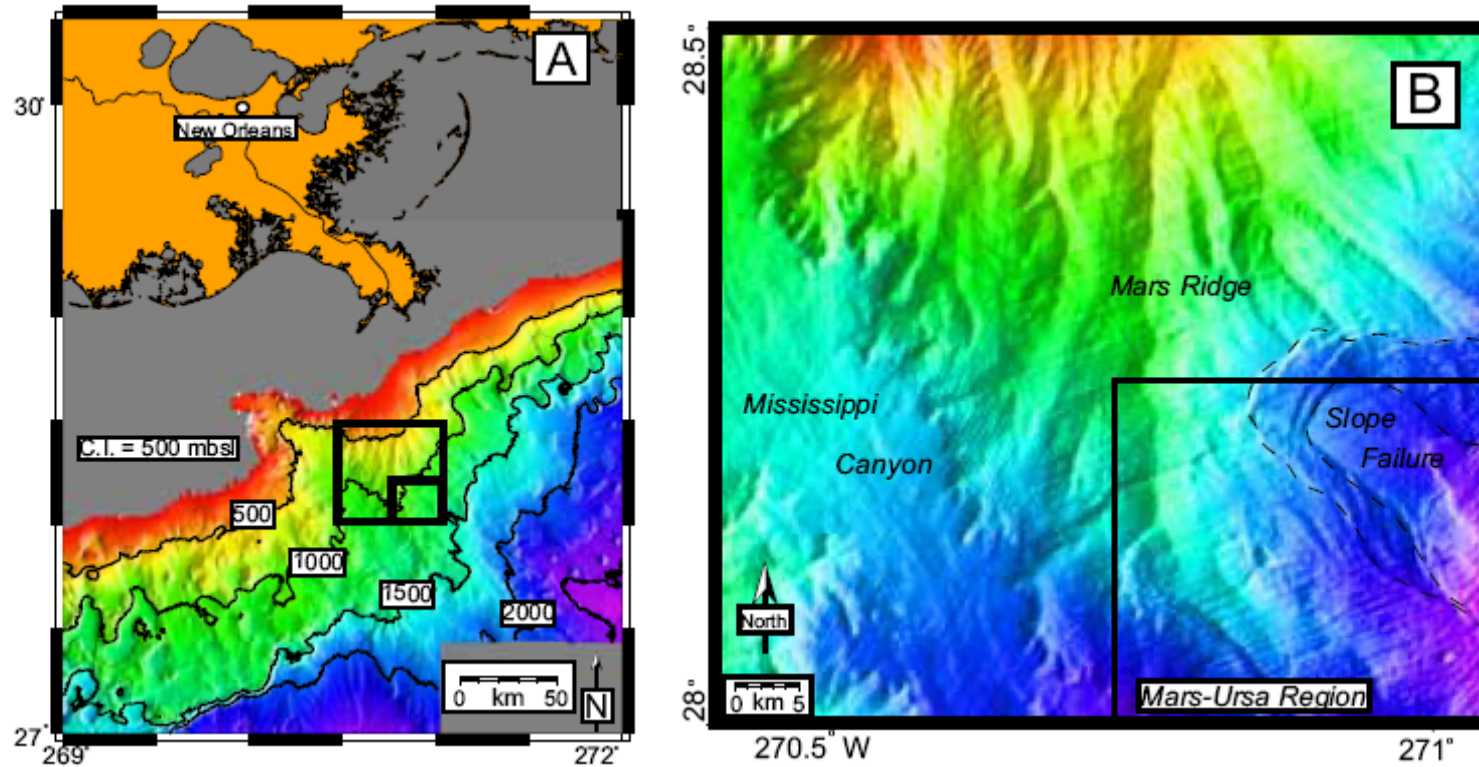
Figure 2-6: A: Base map showing Gulf of Mexico bathymetry and location of Ursa Region. B: Close up of Ursa Region showing the Mississippi Canyon and a submarine slope failure (From Sawyer et al, in press).

Figure 2-7
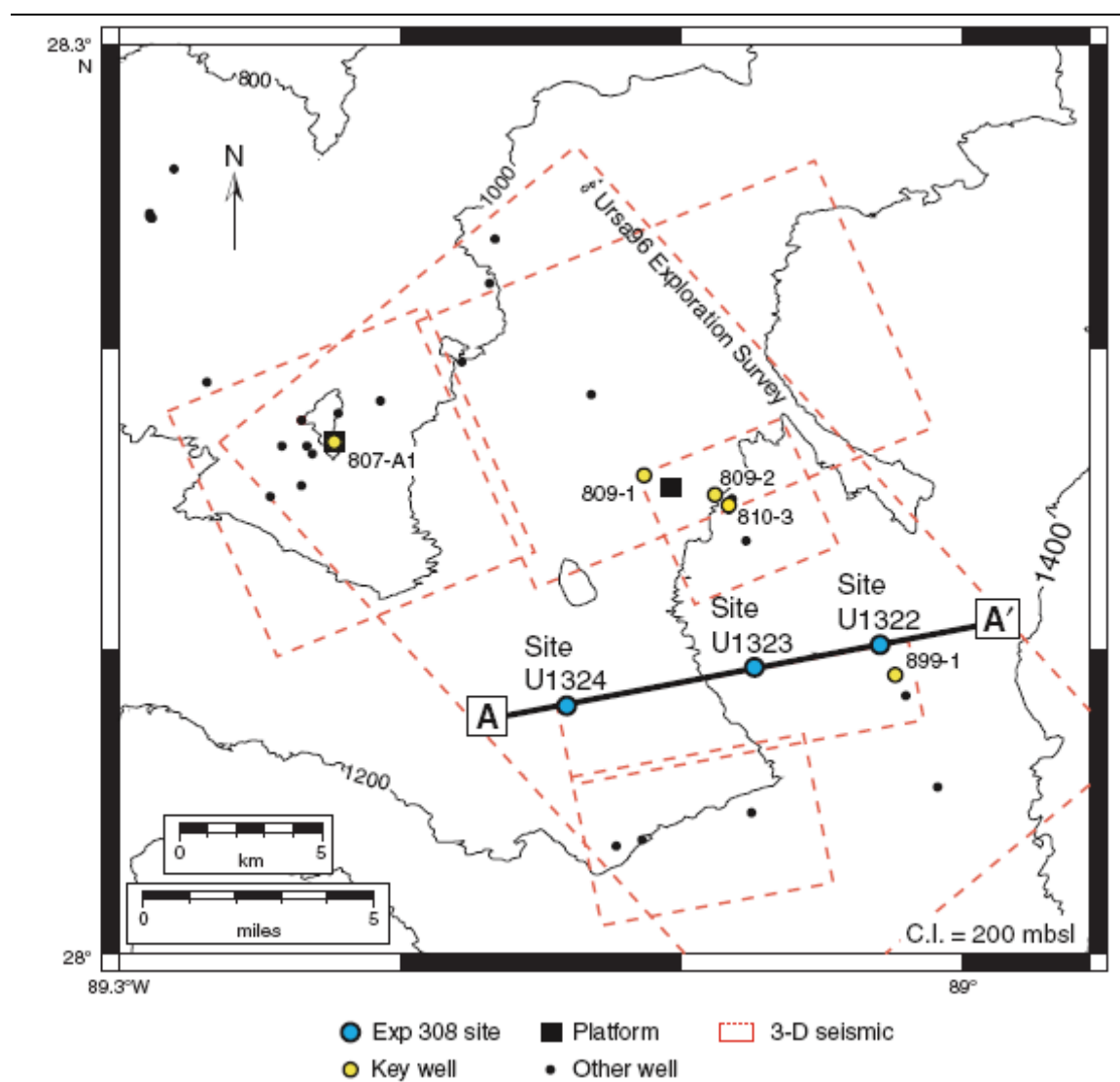
Figure 2-7: Ursa region study area, with survey limits (red lines), reference well 810-3, location of IODP drill sites U1324 and U324, and seismic cross-section A-A' indicated (From Expedition 308 Scientists, 2005).

Figure 2-8
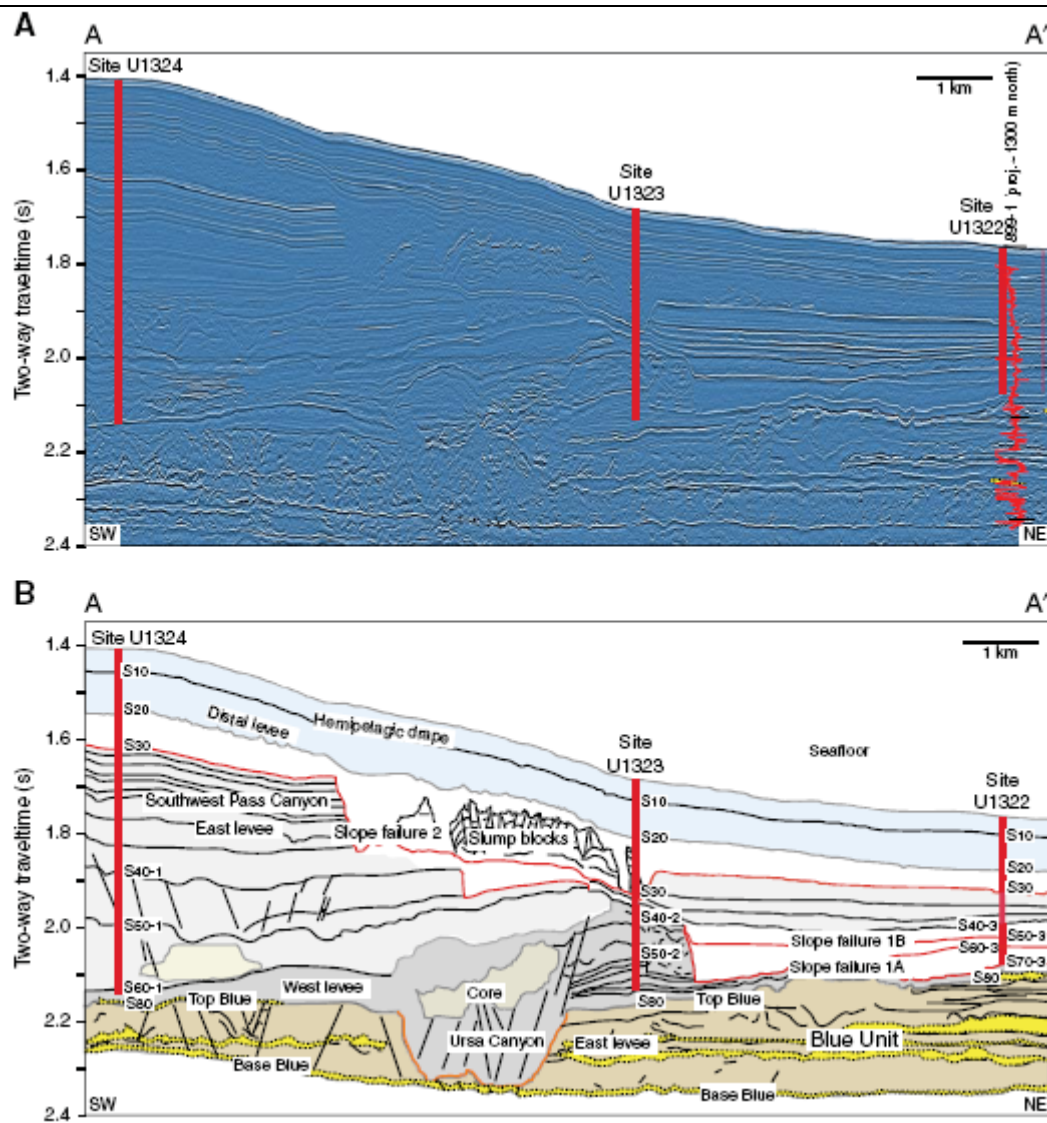
Figure 2-8: Seismic cross-section of Ursa Region showing interpreted sediment facies and major packages simulated in consolidation model. The 1-D Ursa model approximates a vertical section along U1324 (From Expedition 308 Scientists, 2005).

Figure 2-9
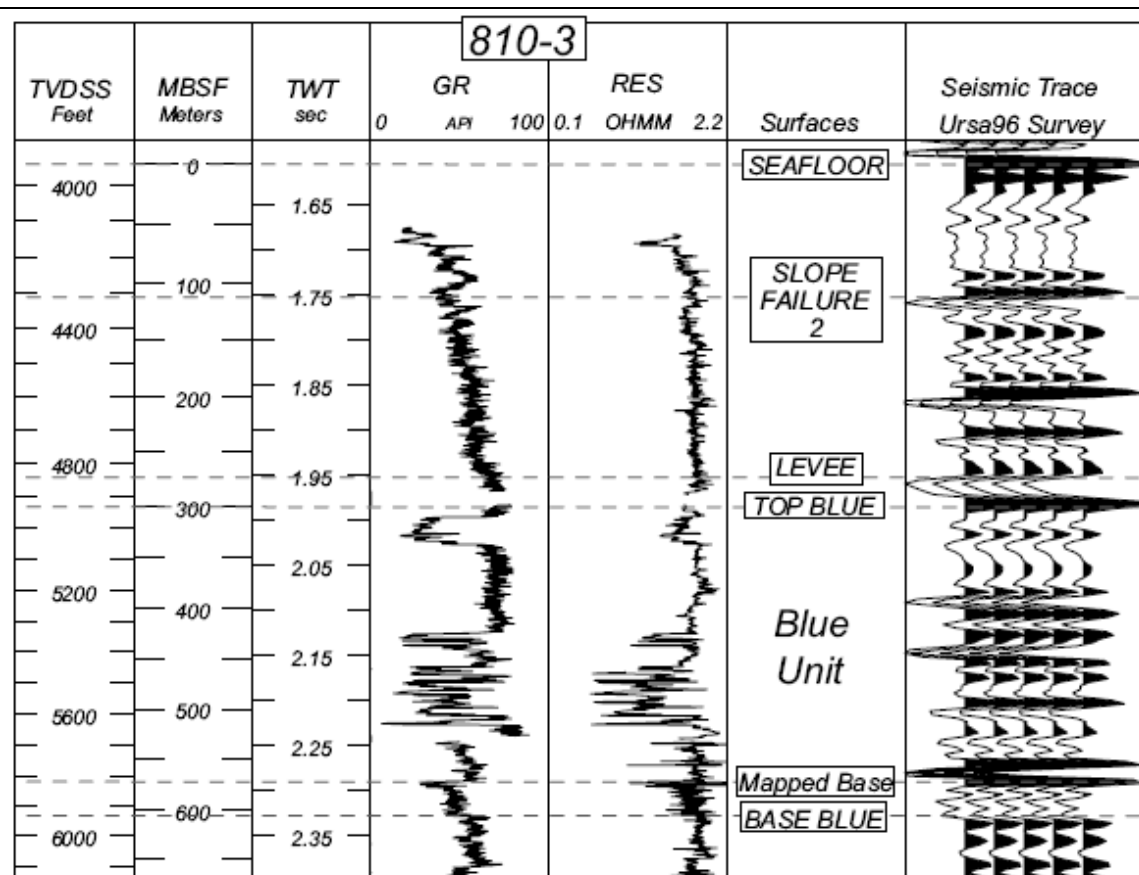
Figure 2-9: A representative well-log showing the gamma-ray (GR) and resistivity (RES) profiles with depth at Well 810-3 in the Ursa Region. The Blue Unit is identified by a significant decrease in the GR and resistivity logs and shows layers of interbedded sand and shales (From Sawyer et al, in press).

Figure 2-10
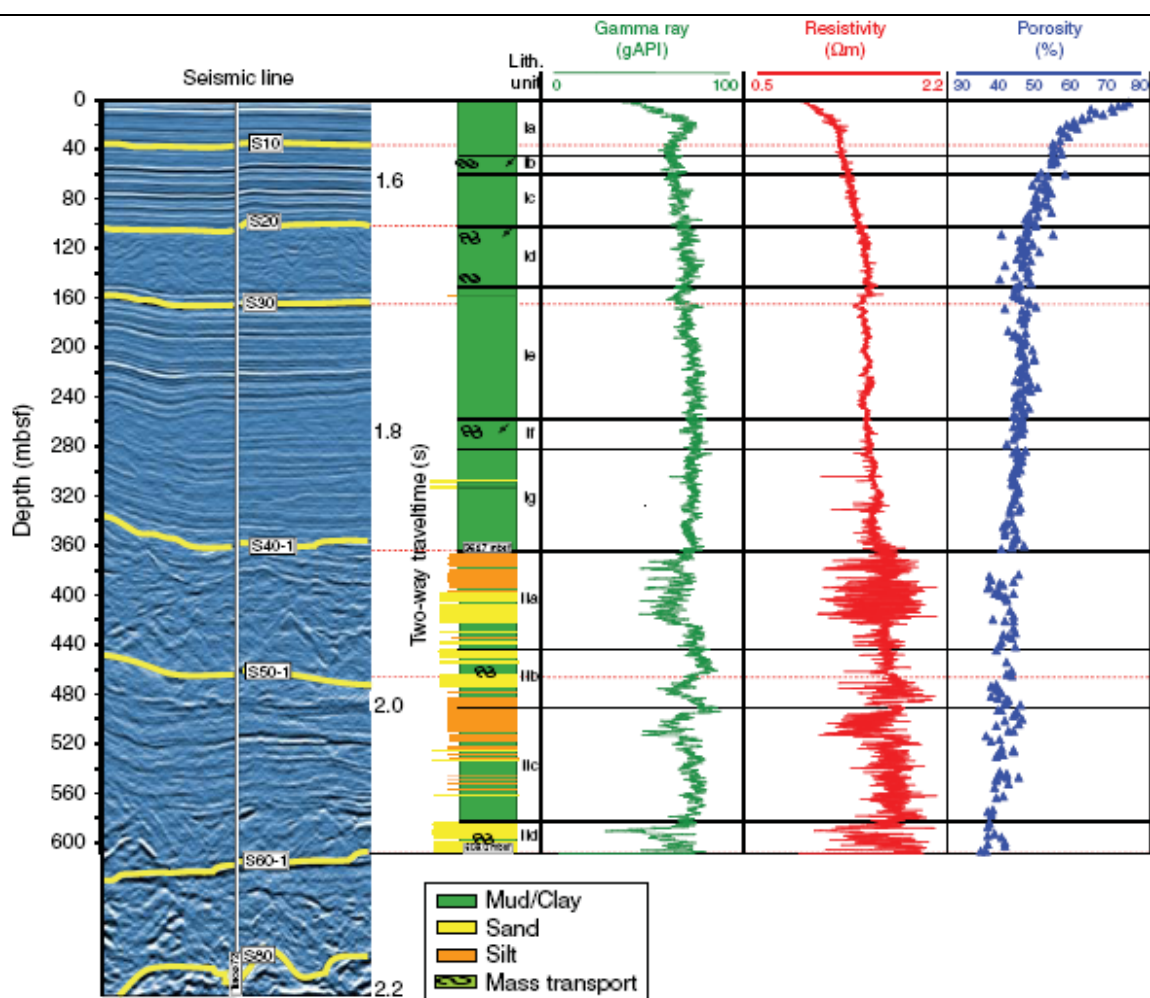
Figure 2-10: Well log from Site U1324 showing gamma ray, resistivity and porosity data for the 600 m of sediment above the Blue Unit at Ursa. A lithology key and seismic line is shown to identify key units (From Expedition 308 Scientists, 2005).

Figure 2-11
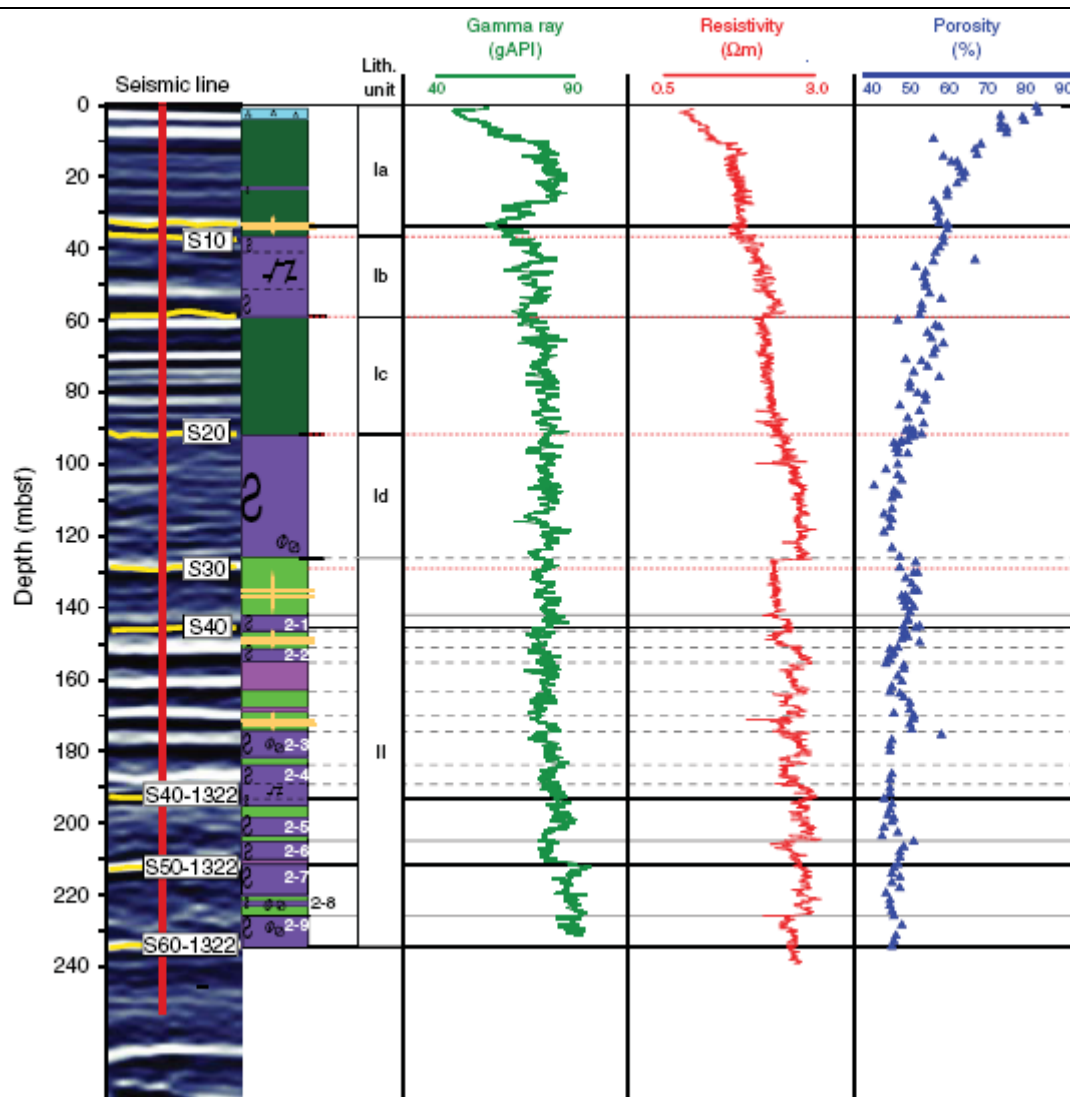
Figure 2-11: Well log from Site U1322 showing gamma ray, resistivity and porosity data for the 240 m of sediment above the Blue Unit at Ursa. An interpreted section of a seismic line is shown to identify key units (From Expedition 308 Scientists, 2005).

2.6 1-D Simulation parameters and Results

Two one-dimensional models of the Ursa Region are constructed as representative vertical sections based on the seismic cross-section and wells U1324 (Figure 2-10) and U1322 (Figure 2-11). The sections consist of four major litho-stratigraphic layers: base shale, Blue Unit, Subunit I and Subunit II. Subunit I (0 – 340 mbsf at Site U1324) is characterized by predominantly mud with some evidence of mass transport deposits. Subunit II is composed of interbedded silt, sand and mud with more frequent traces of mass transport deposits. This lithofacies describes the sediments from 340 mbsf to the top of the Blue Unit at Site U1324.

Simulation constants such as fluid density, viscosity and acceleration due to gravity were listed in Table 2-1. An average grain density of 2.72 g/cc was calculated from the grain density measured at Site U1324.

Layer thicknesses were defined based on the depths measured at Site U1324 (Figure 2-12) and Site U1322 (Figure 2-13). For layers not penetrated by the IODP well, layer thicknesses were estimated from seismic data. The base shale was assigned a thickness of 150 m, which corresponds to 10 ky of sediments accumulating at the sedimentation rate of 0.015 m/yr. As an initial test boundary condition, the base of the model was defined as a no-flow boundary. Fluid flow is laterally restricted in the model by imposing no-flow boundaries on the sides.

Approximate ages for the base of the Blue Unit (70 kya), surface S60 (60 kya) and surface S30 (25 kya), given in the IODP preliminary report, were used to calculate

the sedimentation rates required to produce the existing sediment thicknesses (Table 2-3). The rates are based on the assumption that no significant erosion or compaction occurred. Total simulation time was 80 ky to include deposition of the shale layer below the Blue Unit.

Table 2-3: The Ursa Region models are comprised of multiple layers with varying thicknesses, sedimentation rates and timing of deposition.

Site U1324

Layer	Thickness	Sedimentation Rate	Timing of deposition
Subunit I :			
Seafloor to S20	100 m	0.007 m/yr	0 – 15 kya
S20 – S30	60 m	0.006 m/yr	15 – 25 kya
S30 – S40	180 m	0.014 m/yr	25 – 38 kya
Subunit II :			
S40 – S60	300 m	0.014 m/yr	38 – 60 kya
S60 – S80	30 m	0.006 m/yr	60 – 65 kya
Blue Unit	150 m	0.015 m/yr	60 –70 kya
Base Shale	150 m	0.015 m/yr	70 – 80 kya

Site U1322

Layer	Thickness	Sedimentation Rate	Timing of deposition
Subunit I :			
Seafloor to S20	90 m	0.006 m/yr	0 – 15 kya
S20 – S30	40 m	0.004 m/yr	15 – 25 kya
S30 – S40	20 m	0.002 m/yr	25 – 38 kya
Subunit II :			
S40 – S60	90 m	0.004 m/yr	38 – 60 kya
S60 – S80	10 m	0.002 m/yr	60 – 65 kya
Blue Unit	150 m	0.015 m/yr	60 – 70 kya
Base Shale	150 m	0.015 m/yr	70 – 80 kya

Figure 2-12
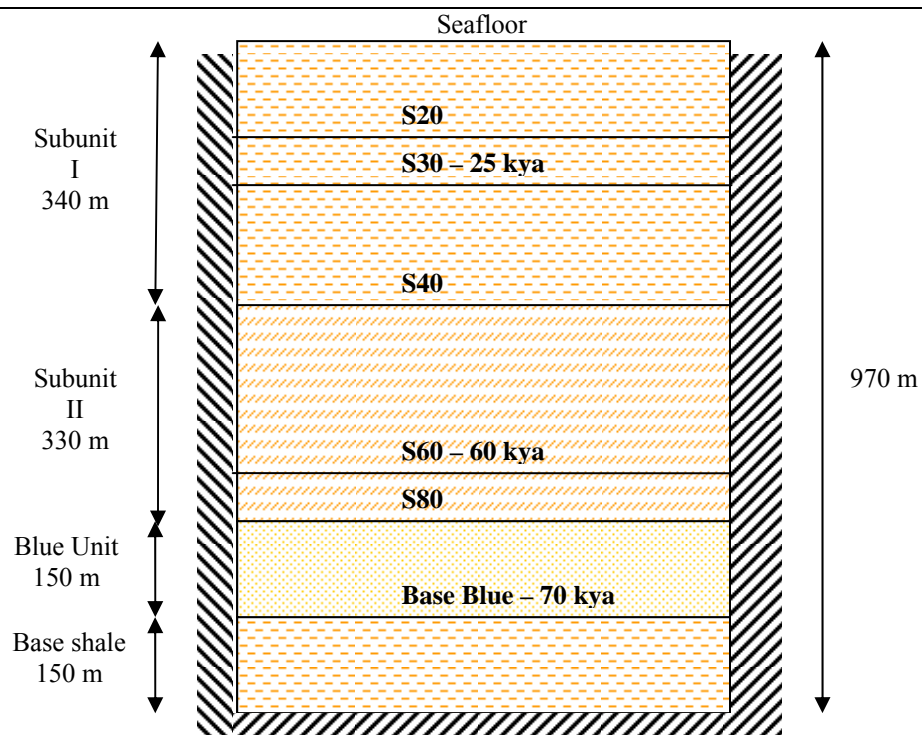
Figure 2-12: A 1-D version of the Ursa Region at Site U1324 is simulated by modeling layers identified from seismic and well-log ties. The seismic surfaces are identified and age dates are given as appropriate. The representative lithofacies used to model the layers are identified at left. Flow is laterally restricted and a no-flow boundary is imposed at the base.

Figure 2-13
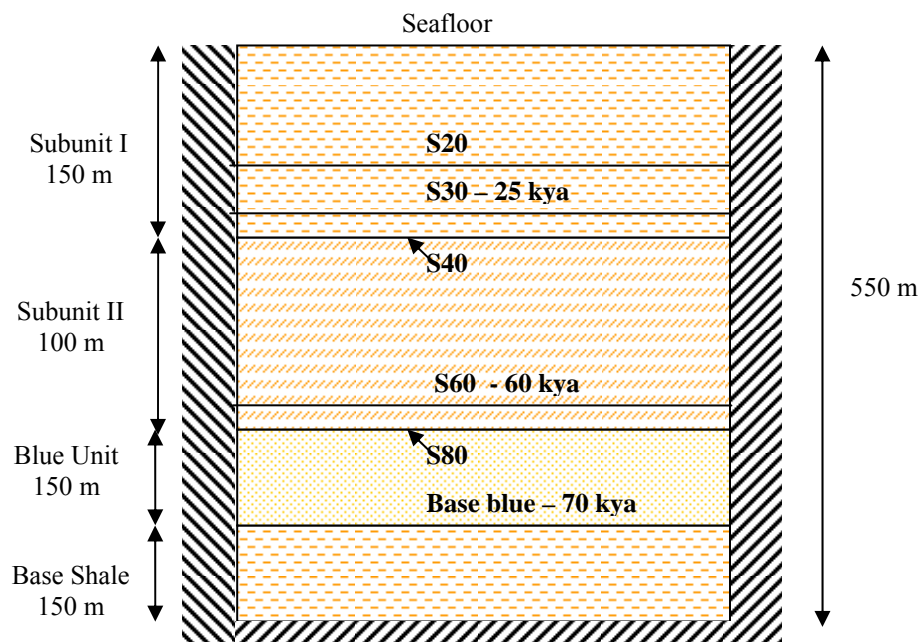
Figure 2-13: A 1-D version of the Ursa Region at Site U1322 is simulated by modeling layers identified from seismic and well-log ties. The seismic surfaces are identified and age dates are given as appropriate. The representative lithofacies used to model the layers are identified at left. Flow is laterally restricted and a no-flow boundary is imposed at the base.

2.6.1 Porosity-Effective Stress Relationship

To determine a porosity-effective stress relationship for the Ursa Region, data from IODP Expedition 308 well U1324 was used. Porosity was determined from moisture and density testing on 10 cc core plugs (Expedition 308 Scientists, 2005). Bulk density was measured at Site U1324 using a wireline logging tool. The overburden stress is calculated by integration of the bulk density log. The shallow section (35 – 105 mbsf) is assumed to be hydrostatically pressured and the (hydrostatic) effective stress is calculated by subtracting hydrostatic pressure from the overburden stress. Following the method of Hart et al (1995), a plot of log porosity against hydrostatic effective stress is used to constrain the values of initial porosity and bulk compressibility (Figure 2-14). A least squares regression is used to determine the equation that best fits the data. The slope of the line provides the bulk compressibility, while the intercept gives the value of initial porosity. By this method, we obtain a bulk compressibility value of 1.48×10^{-7} Pa^{-1}, and an initial porosity value of 0.61.

Figure 2-14
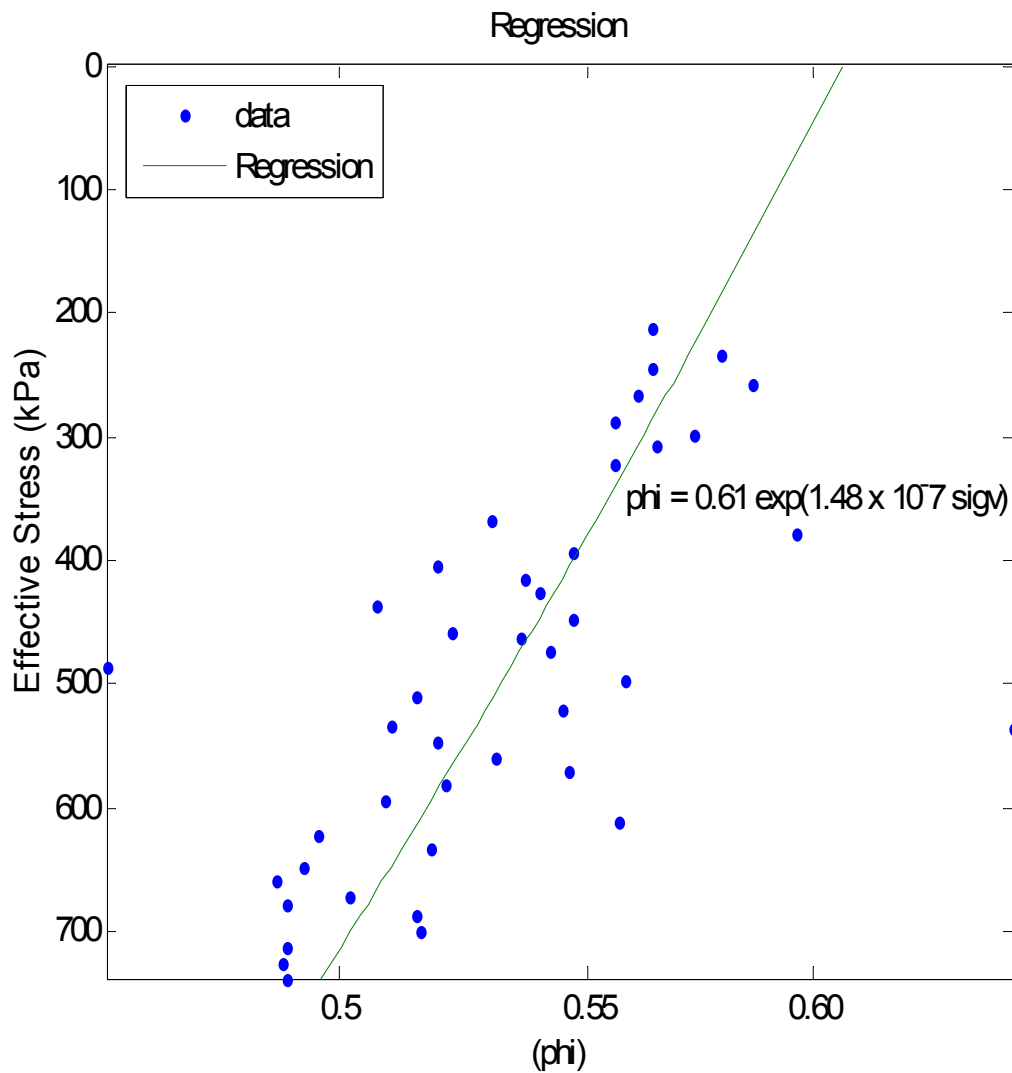
Figure 2-14: Least squares fit of effective stress versus log porosity of sediments in the shallow (35 – 105 mbsf) hydrostatically pressured region of U1324 is used to determine sediment properties. The slope of the line provides the estimate of matrix compressibility, and intercept gives initial porosity for the Ursa Region.

2.6.2 Permeability Models

The lithology and permeability of the Ursa Basin was characterized using representative permeability-porosity functions for the lithological layers defined from seismic and core descriptions. Consolidation experiments on saturated core samples from several depths at Site U1324 were performed to determine the relationship between hydraulic conductivity and porosity for the Ursa sediments (Long, 2006). These relationships are listed in Table 2-4. Hydraulic conductivity, K_s, is calculated as the intrinsic permeability of the sediments divided by the dynamic viscosity of the fluid.

$$K_s = \frac{k}{\mu}.$$

(2.16)

The relationships between hydraulic conductivity and porosity were used to determine representative porosity-permeability relationships for the Ursa Region sediments. These relationships were used to approximate Subunit I and Subunit II lithofacies (Figure 2-15). The base shale layer was modeled using the Subunit I function.

For the Blue Unit, a permeability function derived by Flemings et al. (2001) for the Bullwinkle sands was adopted. This permeability relationship, given below, applies when permeability is measured in darcies. (A conversion factor of 1 mD = 9.869 x 10^{-16} m^2 is used).

$$Log\ k = 10.8\varphi - 0.7.$$

(2.17)

Table 2-4: Hydraulic conductivity relationships determined from consolidation experiments on Ursa sediments at different depths from Site U1324 (Long, 2006).

Core Depth (mbsf)	Stratigraphic layer	Hydraulic Conductivity Function
51	Subunit I	$K_s = 4.148 \times 10^{-15} (\exp(\frac{\phi}{0.112(1-\phi)}))$
577	Subunit II	$K_s = 1.513 \times 10^{-14} (\exp(\frac{\phi}{0.1015(1-\phi)}))$

Figure 2-15
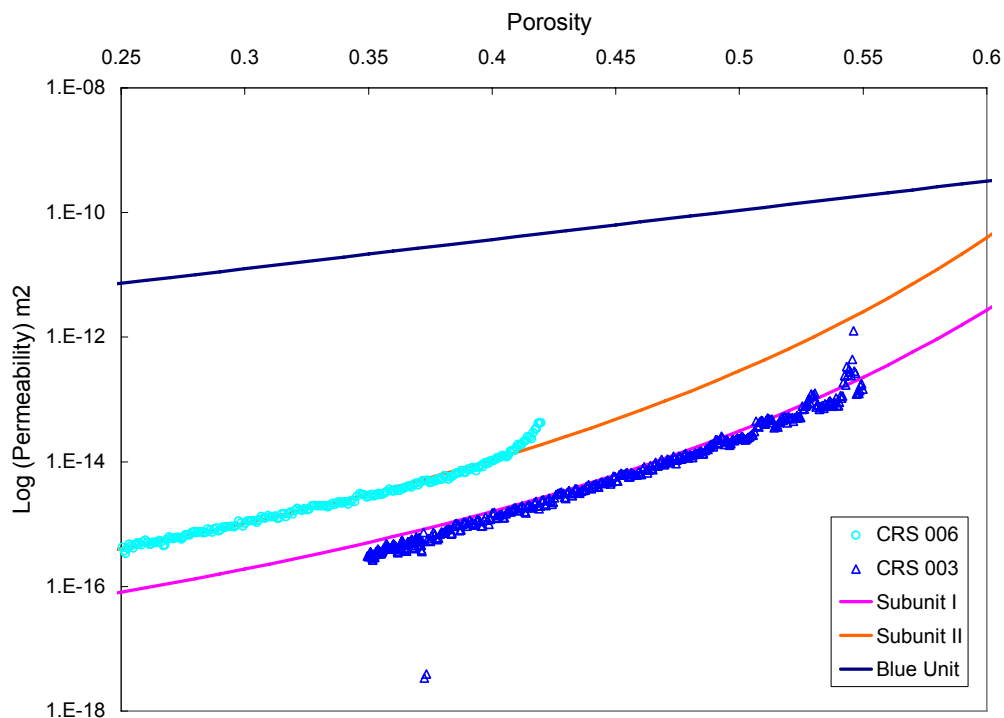
Figure 2-15: Permeability functions used in the simulation of Ursa Region sediments in Subunit I (purple line) and Subunit II (orange line) are shown on a semi-log plot. The functions are derived from data from consolidation experiments on 2 Ursa core samples – CRS003 and CRS006 (Long, 2006) shown using symbols. The Blue Unit (blue line) is simulated using a permeability function developed for the Bullwinkle sand (Flemings et al., 2001).

2.6.3 Results

The model reports onset of overpressure within 50 mbsf. This shallow overpressure overpredicts IODP estimates above 200 mbsf. Above this depth, the IODP predicts hydrostatic pressures. Between 200 – 400 mbsf, overpressures closely approach the IODP estimates and give a good match to the data in the upper 400 mbsf. Below 400 mbsf, the Matlab® model predicts only 80% of the overpressure estimated by the IODP (Figure 2-16).

Change in the gradient of the overpressure is closely matched to the boundaries of the lithofacies which are identified on the porosity and permeability plots on the right of Figure 2-16. Overburden stress predicted by the Matlab® model slightly underpredicts the IODP data. This indicates that the solid fraction deposited in this simulation is less than that observed at Site 1324.

Figure 2-16
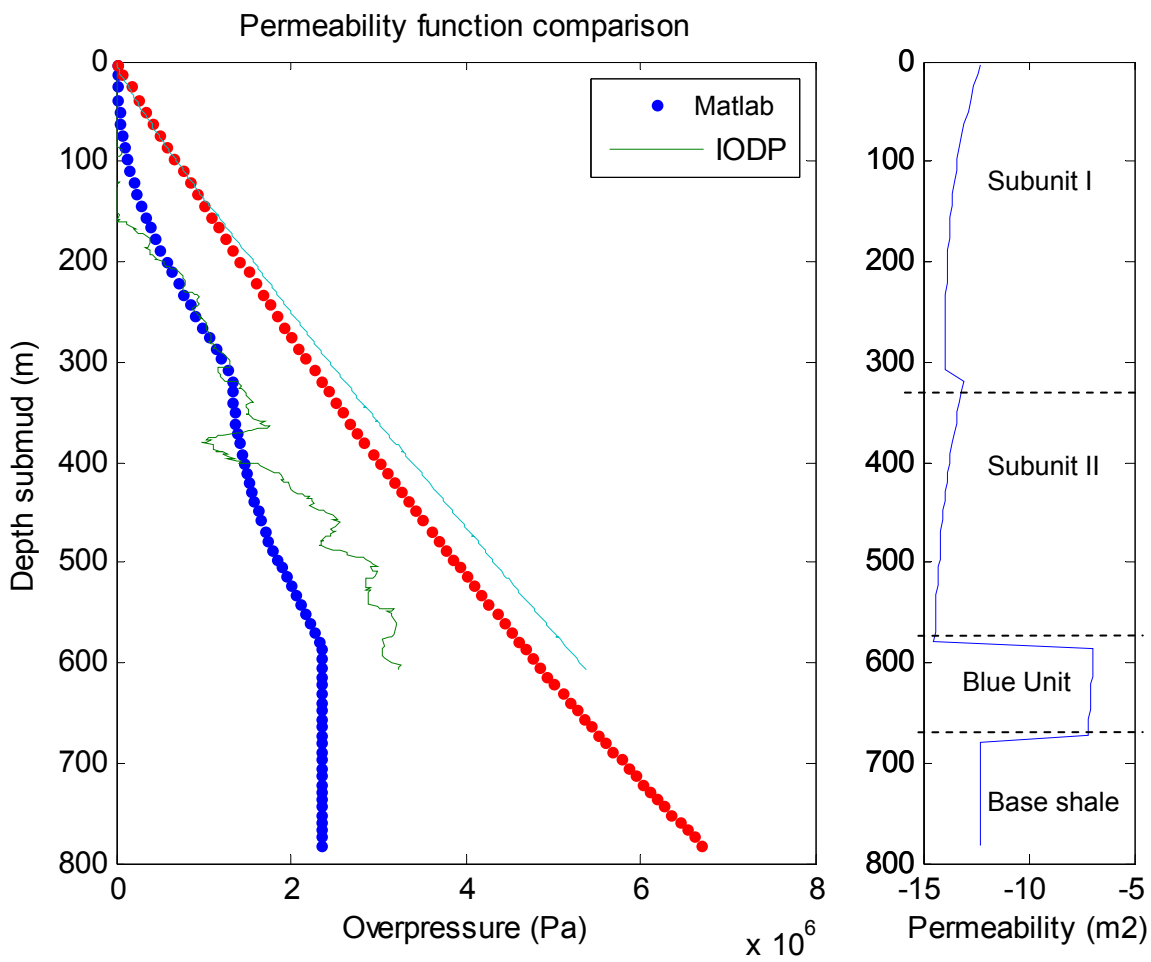
Figure 2-16: Overpressure and reduced lithostatic stress predicted using the Matlab model (dotted lines) underpredict the IODP estimates (solid lines) for Site U1324. The permeability profile used in the simulation is shown on the right, and lithology layers are labeled.

2.7 Discussion

Comparison with analytical solutions

Two analytical solutions are compared with the numerical 1-D consolidation model. Close agreement with Turcotte and Schubert's analytical solution of the diffusion equation indicates that the diffusive component is correctly discretized. However, the solutions are not identical as the Matlab® model allows for build-up of strain, which is not accounted for in the analytical solution. The Matlab® model converged on the analytical solution during low permeability simulations, or when there is the least amount of strain.

In the comparison with the Gibson consolidation solution, the Matlab® model showed the best agreement with large time factors. Large time factors occur with fast sedimentation rates and/or with low permeability sediments. This is an encouraging result as the Gibson model was developed for consolidation of low permeability clays, or low-strain simulations. In the Gibson solution, bulk density and compressibility are specified constant over the simulation period, while the bulk density is allowed to vary with overpressure in the numerical model. Additionally, the Gibson solution is based on compaction of clays over a very small depth range or small change in effective stress. The model domain and parameter values for the Matlab® model can be significantly larger with depths of several kilometers and large variations in effective stress.

The Gibson solution, due to its constant permeability and compressibility requirement, cannot accurately model rapid consolidation in shallow submarine

sediments, as in the Ursa Region. At these depths and large effective stress ranges, a Matlab® model is required to simulate the complexities of sub-sea consolidation, where large strain accumulates.

Ursa simulation results

The Ursa simulation produced overpressures that closely approached the IODP data in the uppermost 400 mbsf. However, this model overpredicted the overpressures in the shallow region above 200 mbsf. At depths below 400 mbsf, the model underpredicted the IODP estimates, particularly at the depth of the Subunit II layer. This may indicate that the sedimentation rates for this layer are too slow. The interpreted seismic cross-section suggests that this layer experienced significant post-depositional erosion. Some correction, to factor in the effect of higher sedimentation and later erosion, may be necessary to improve the overpressure prediction for this layer.

An alternative source of error may be that the permeability function used does not adequately reflect the permeability of the sediments. The simulation was run with single permeability functions over layers several hundred meters thick. Permeability was also assumed to be isotropic. The sediments may be less permeable or more simply, less connected laterally due to erosion. To improve the predictive ability of the 1-D model, alternative permeability profiles may need to be considered. Additional testing with multiple permeability functions and varying degrees of anisotropy may produce more accurate pressure profiles.

With multiple layers and multiple permeability functions, averaging techniques have been used to approximate the layering effect of mixed lithologies. The averaging

methods control the weighting of individual constituent permeabilities as well as the degree of anisotropy in the mixed layer. Empirical testing, in other models involving shale sediments with small sand percentages, provides support for the use of horizontal geometrical averaging of end member permeabilities. In the vertical direction, harmonic averaging is used to represent the decreased diffusivity of such mixtures (Fogg, 1986; Harrison and Summa, 1991).

Additional boundary conditions can also be considered. A no-flow boundary condition was imposed at the base in both 1-D models and this may not be a true reflection of the flow conditions in the Ursa sediments. High overpressure at Ursa suggests a regional aquifer may drive flow through the system and feed overpressure, particularly in the Blue Unit. Additional runs with alternative overpressure boundary conditions may improve the match between simulation results and IODP data and provide support for the regional aquifer model.

Chapter 3

Multi-dimensional Compaction flow modeling of Ursa Region

3.1 Abstract

Compaction results from the Stellar™ model and the Matlab® model of the previous chapter agree closely. However, one- and two-dimensional Ursa simulation results using Stellar™ overpredict the pressure estimates from the Integrated Ocean Drilling Program (IOPD) Expedition 308 at shallow depths (< 200 mbsf). The Stellar™ models show close agreement with the IODP data only at depths greater 200 mbsf. At shallower depths, the Stellar™ models predict significant overpressure where IODP overpressure estimates hydrostatic pressure conditions. The two-dimensional models show that the overpressure decreases from west to east and fluid flow is focused within the Blue Unit sands. Extractions of overpressure at different times show that the most significant overpressure is generated in the last 30 kya, while the Subunit I lithofacies is deposited.

3.2 Introduction

The Stellar™ numerical model is a proprietary finite-difference model that solves the diffusion equation in three dimensions. The model solves the partial differential equation describing fluid flow and compaction as described in Chen et al (2002).

$$\frac{\partial(\rho_f \phi)}{\partial t} = -\nabla \cdot (\rho_f u_s) + \nabla \cdot \left(\frac{\rho_f}{\mu} k \nabla P^* \right) + q \ . \tag{3.1}$$

In the equation above, u_s is velocity of the compacting medium and q is the source or sink term.

The basin model is built with geometric layers defined by height, width and length or, by finite surfaces derived from surface and isopach maps. These layers and surfaces are assigned lithological properties such as permeability, porosity and anisotropy. Porosity and permeability can be defined as constants, or expressed as exponential functions.

Porosity is calculated as an effective stress dependent function.

$$\phi = \phi_0 e^{\left(-\beta_s \sigma_v^{'}\right)} \ . \tag{3.2}$$

The permeability function is a modified form of the Carman-Koseny function:

$$k = k_0 \frac{(1-\phi_0)^m}{\phi_0^n} \frac{\phi^n}{(1-\phi)^m} \ . \tag{3.3}$$

The values of k_0 are specified according to constant permeabilities defined in the previous chapter. Values of m and n are determined using curve matching to produce permeability relationships that approximate the functions given in Chapter 2 (Figure 3-1) and are listed

in Table 3-1. The Carman-Kozeny functions agree closely with the exponential functions for porosity values above 35% for Subunit II and above 45% for Subunit I. This is within the range of measured porosity (40 – 61 %) for Ursa sediments above 1000 mbsf. These porosity values are low for shallow sediments, but are the experimentally determined porosity values from the regression in Figure 2-14 .

Figure 3-1
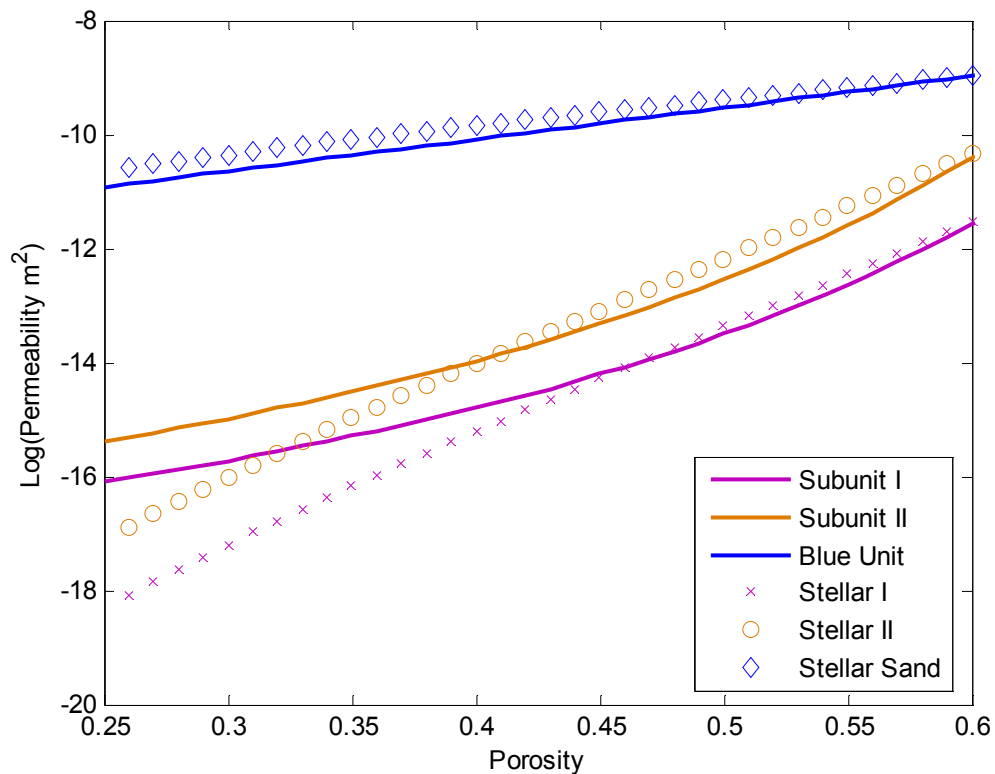
Figure 3-1: Plot showing the match between Stellar™ permeability functions (symbols) and the exponential functions (solid lines) from Figure 2-15 used in the Matlab® model of Chapter 2. The permeability functions show good agreement for porosities higher than 35 % for Subunit II (Stellar II) and higher than 40 % for Subunit I (Stellar I). Stellar Sand models the permeability function used to represent the Blue Unit.

Table 3-1

Table 3-1: Permeability exponents used in Stellar function

Layer	m exponent	n exponent
Subunit I	11	10
Subunit II	11	10
Blue Unit	2	3

Although the onset and duration of deposition is specified in the model, the geometry of the present day sediment column is also defined. This present-day geometry, in terms of layer thicknesses, is used to verify model results. The forward model estimates the amount of sediment deposited during the simulation. If the predicted final layer thicknesses conflict with the present-day geometry, the model is repeated varying the amount of sediment deposited until the error in layer thickness is less than 1 %.

The Stellar™ model can be used to characterize and simulate basins in 1-, 2- and 3-dimensional runs. The model is compared with the Matlab® model of Chapter 2 for verification, and then to overpressure estimates from the IODP Expedition 308. The intent is to simulate the Ursa Region in order to define the flow regime and pore pressures in multiple dimensions.

To validate the Stellar™ model, simple 1-D models are run to compare the simulation output with the Matlab® model. A single Carman-Koseny type permeability function is used in all the layers. The function is adjusted by varying the initial permeability (k_0) values in Equation 3.3. The k_0 values used are: 4.818×10^{-18} m^2 (0.005 md) and 4.818×10^{-15} m^2 (4.88 md). The latter is the representative shale permeability in the Ursa simulation, while the former simulates relatively impermeable sediment. Initial

porosity (φ_0) is 0.61 in both simulations. Values for *m* and *n* used in this test are 4 and 5 respectively. The simulations are allowed to run for 80 ky with a constant sedimentation rate of 0.015 m/yr.

Simulation results between the Stellar™ and the Matlab® model agree (Figure 3-2), although there is a difference in the overall thickness of sediment deposited. Note that all the Stellar™ results show the same end thickness of sediment deposited (900 m). In the Matlab® model, however, the total sediment column is shorter (or more compacted) in the higher permeability run. The converse is true for the lower permeability run.

For the shale permeability simulations (k_0 = 4.88 mD), both models show a near hydrostatic condition in the upper 200 mbsf, with a gradual increase in overpressure with depth. For the low permeability (k_0 = 0.005 mD) runs, the simulations again agree. The overpressure generated is very close to the reduced overburden stress, and the overpressure begins within 50 mbsf.

Figure 3-2
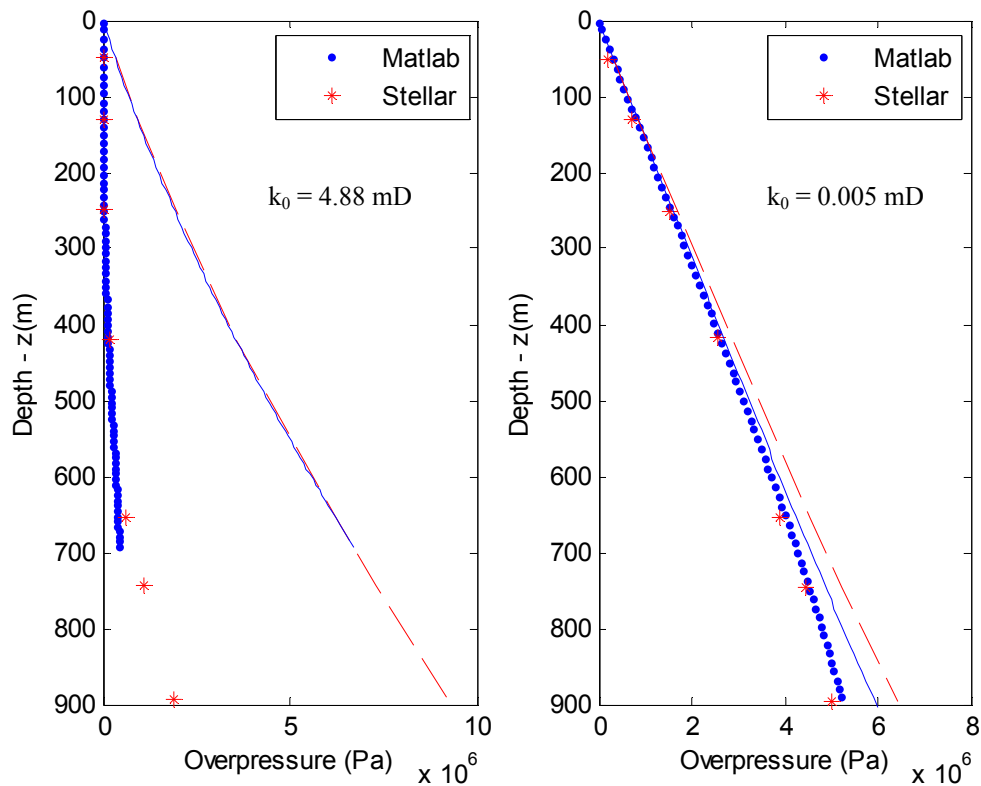
Figure 3-2: Stellar™ models are run using a single Carman-Kozeny type permeability function in all layers and compared with the Matlab® model. The functions are modified by changing the initial permeability (k_0) values, which are labeled on the graphs. Stellar results (red *'s) agree with the Matlab® model (blue dots) for both permeability tests. Model inputs are described in Section 3.2.

3.3 1-D Ursa model

The 1-D consolidation model is built of 7 layers with thicknesses as prescribed in Figure 2-12 for Site U1324 and Figure 2-13 for Site U1322. The depositional ages of the layers as defined in Table 2-3. Lithofacies are defined using the Carman-Kozeny adaptations of the permeability functions presented in Chapter 2 and shown graphically in Figure 3-1. The simulation is run for 80 ky.

Lateral boundaries and the base of the sediment column are set to be no flow boundaries. As lithology is laterally uniform, the flow field is vertical only. Pressure results are presented at grid cell centers.

3.3.1 Results

The Stellar™ 1-D model of Site U1324 produces overpressures that overpredict the overpressure estimates from the IODP data in the uppermost 150 mbsf. The model diverges from the hydrostatic and predicts significant overpressure within 100 mbsf (Figure 3-3). The IODP estimates indicate a hydrostatic condition to 150 mbsf. At depths greater than 200 mbsf, the model agrees with the IODP estimates and even underpredicts the estimates at depths below 500 mbsf. The Blue Unit is predicted to be moderately overpressured with an overpressure ratio (λ^*) of 30 %.

At Site U1322, the Stellar™ 1-D model again overpredicts the overpressure estimates from the IODP data. In the uppermost 150 mbsf, the model predicts a moderate

overpressure where the IODP data shows hydrostatic pressures (Figure 3-4). Onset of overpressure is predicted again within 50 mbsf, which is almost 100 m above the IODP onset point. At depths greater than 200 mbsf, the model agrees with the IODP estimates.

Figure 3-3
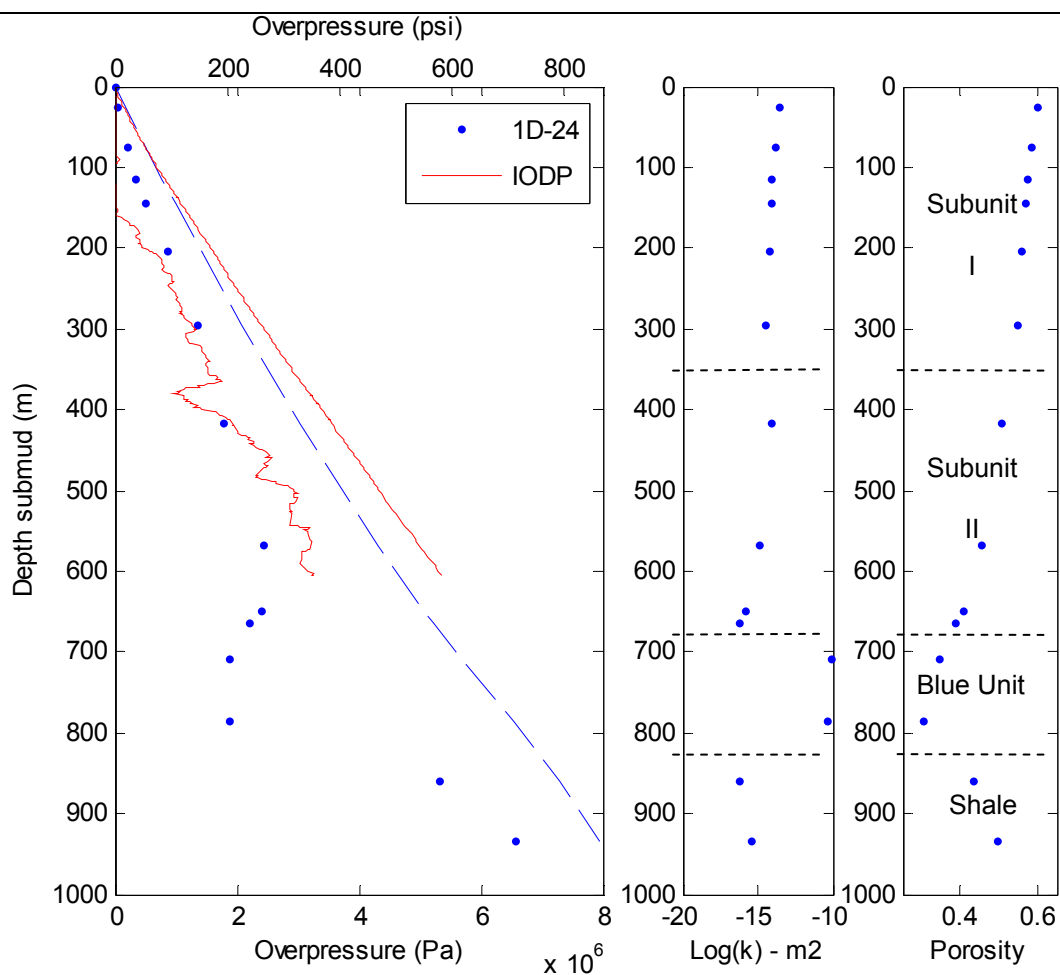
Figure 3-3: Simulation results from the Stellar™ 1-D model of Site U1324 using permeability functions (1D-24 = blue dashed line) overpredicts the IODP overpressure estimates (IODP = red solid line) for layers above 400 mbsf. Lithology layers are labeled on the permeability and porosity plots on the right. Inputs are described in Section 3.3.

Figure 3-4
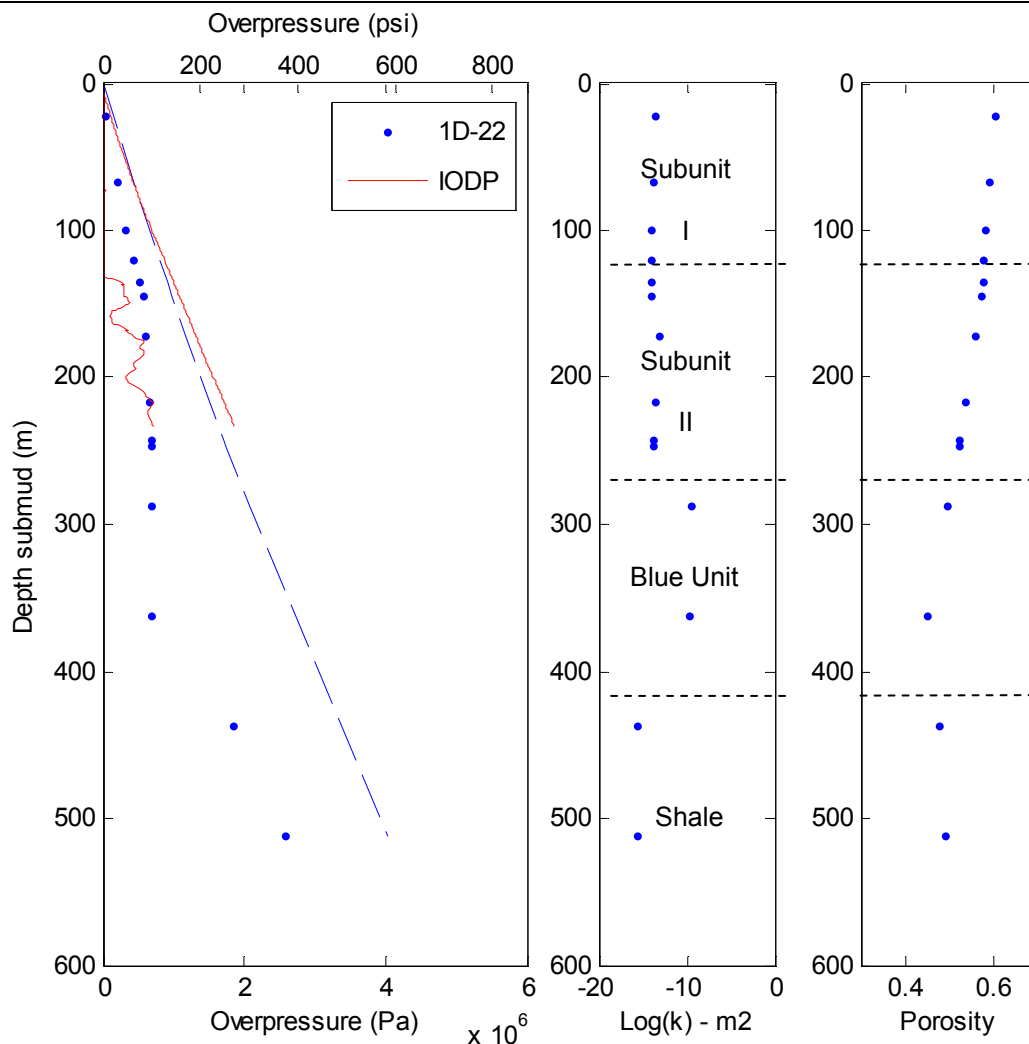
Figure 3-4: Simulation results from the Stellar™ 1-D model of Site U1322 (1D-22 = blue dashed line) show significant overpressure development after 80 ky of sedimentation. The model overpredicts the IODP overpressure estimates (IODP = red solid line) above 175 mbsf. Permeability and porosity are shown at right, with lithofacies labeled. Inputs are described in Section 3.3.

3.4 2-D Ursa model

This model is built from a geometric adaptation of the seismic cross-section, which illustrates the wedge shaped nature of the Ursa Region deposits (Figure 3-5). Isopachs showing the lateral variation in the east-west direction are constructed for each layer. Thicknesses are pegged to the observed layer thicknesses from Site U1324 and Site U1322. Elsewhere in the section, layer thicknesses are estimated from the seismic cross-section. These isopachs are assigned the same depositional history as the constant thickness layers defined in Table 2-3. Lithofacies are defined using the Carman-Kozeny adaptaptions of the permeability functions defined in Chapter 2 and presented graphically in Figure 3-1. The simulation is run for a total of 80 ky.

Boundaries are closed at the base and the sides. The only open flow boundary is at the surface. Therefore, flow is constrained to the east-west and vertical directions only. The objective is to identify whether fluid flow is being driven towards the toe of the wedge as predicted by flow focusing models (Dugan and Flemings, 2000; Lupa, 2002; Flemings et al, 2002).

Overpressure, effective stress and overpressure ratio results are presented as 2-D cross-sections for the region highlighted by the red box in Figure 3-5. Additionally, 1-D equivalent extractions were made for Sites U1324 and Site U1322 and are compared with the IODP estimates. These results are also compared to the previous 1-D model results. All results are presented at the grid cell centers.

Figure 3-5
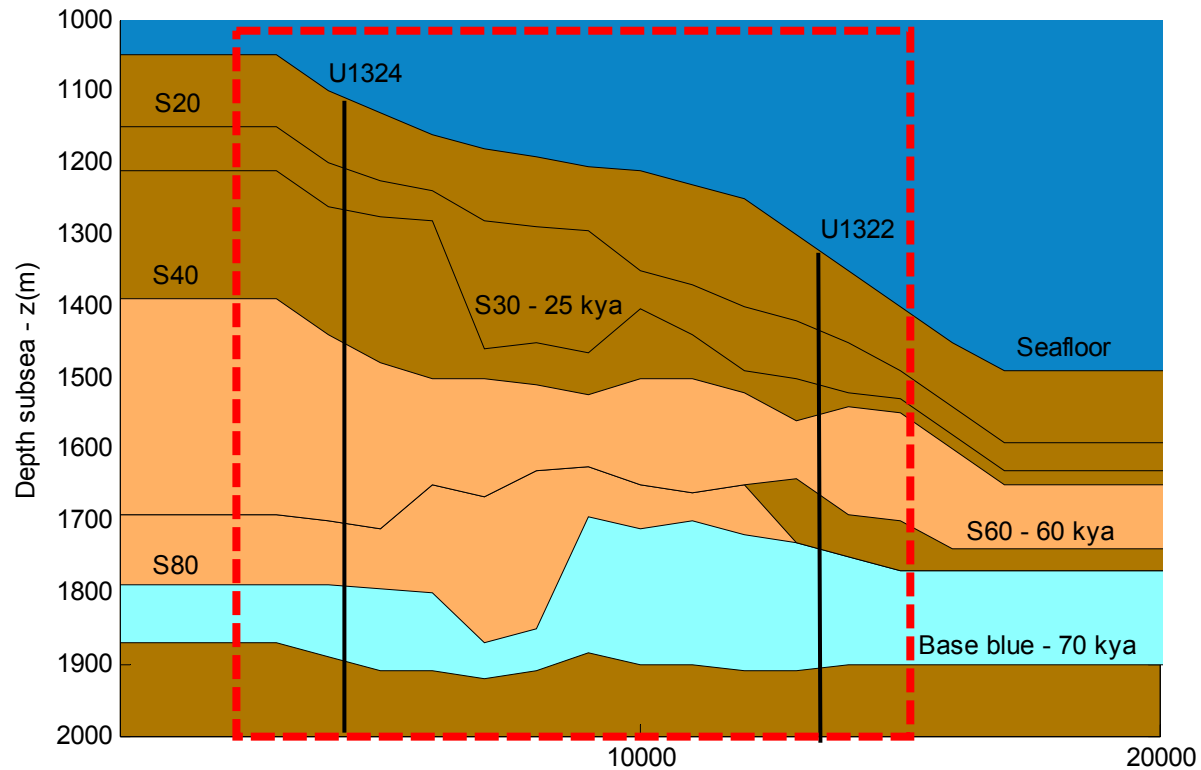
Figure 3-5: Simplified cross-section of the Ursa region is used in the Stellar 2-D model. Key seismic surfaces and age dates are highlighted. Colors identify the lithofacies used in the simulation, where brown is Subunit I, orange is Subunit II and blue is the Blue Unit. Results from the 2-D model are shown for the region highlighted by the red box. Extractions for Sites U1324 and U1322 are taken at the location of the solid black lines.

3.4.1 Results

Overpressures from the 2-D Stellar simulation decrease from west to east, and from the base towards the surface (Figure 3-6). The pressure gradient is most significant in the shale below the Blue Unit (third and fourth layers from the base) and in the Southwest Pass Canyon sediments (seventh and eighth layers from the base). The pressure gradient in the Ursa sediments drives fluid toward the east where the sediment package thins. The variation in overpressure above and below the Blue Unit is also likely to drive fluids into the Blue Unit, where the higher permeability sands allow for high flow velocities.

Effective stress also decreases from west to east in accordance with the thinning of the sediment package (Figure 3-7). The highest effective stress is observed at the western end of the Blue Unit layers (third and fourth layers from the base), which is an indication that the overpressures are low in this location. This is also evident in the overpressure ratio (λ^*) cross-section, which records low λ^* values in the Blue Unit (Figure 3-8). The maximum λ^* equal to 0.90 occurs in the toe of the wedge to the east of Site U1322. The base shale, bottom two layers, also shows an elevated λ^* of 0.80. The base shale also has the lowest permeability of the section (Figure 3-9). The Blue Unit has the highest permeability and is shown in red.

Extracted 1-D results from Site U1324 for the permeability-function model indicate that the overpressure again overpredicts the IODP estimates at depths above 150 mbsf (Figure 3-10). As in the 1-D model, the overpressure is similar to the IODP

estimates at depths between 200 – 500 mbsf. Below 500 mbsf, the model underpredicts the IODP estimates. The 2-D model results are nearly identical to the 1-D models at site U1324 (Figure 3-11).

Extracted results at Site U1322 show overpressures that again overpredict the IODP estimates (Figure 3-12). This result is much higher than the IODP estimates throughout the sediment column. The overpressures from this 2-D extraction are also higher than that of the 1-D model of Site U1322 (Figure 3-13). The largest increase in overpressure is observed in the Blue Unit layers and above. This higher overpressure in the 2-D model may be evidence of flow towards Site U1322.

Figure 3-14 and Figure 3-15 show the change in overpressure as the layers are deposited in time. Significant overpressures begin to be generated in the last 30 ky when Subunit I lithofacies is deposited (Figure 3-15). The largest overpressures are seen in the present day in the basal shale layers (bottom two layers). Comparison of extractions from the 2-D model at Site U1324 for the present day and 40 kya indicate that little overpressure was maintained in the sediments above the Base Shale at that time (Figure 3-16).

Figure 3-6
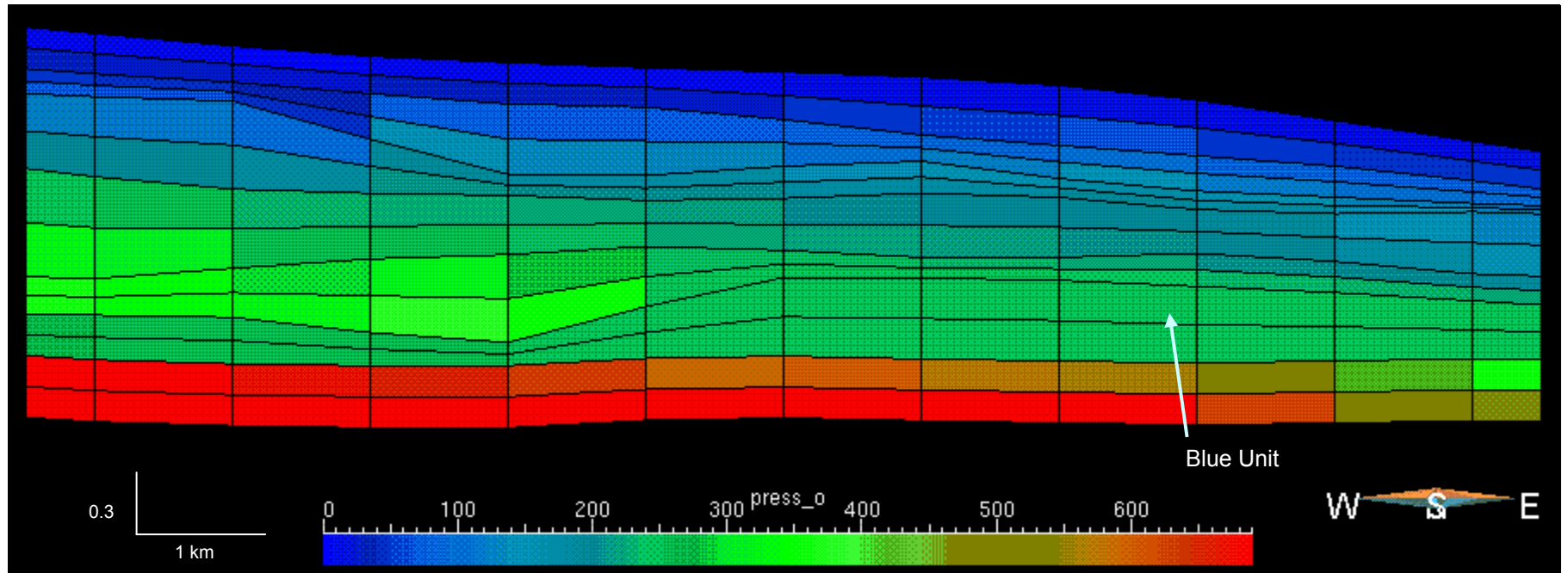
Figure 3-6: Overpressure (in psi) from the Stellar 2-D simulation is shown in cross-section after 80 ky of simulation. Overpressure decreases from left to right and from base of column to sea floor. The location of the Blue Unit (third and fourth layers from the base) is highlighted. Cell boundaries are shown in black. Model inputs are described in Section 3.4.

Figure 3-7
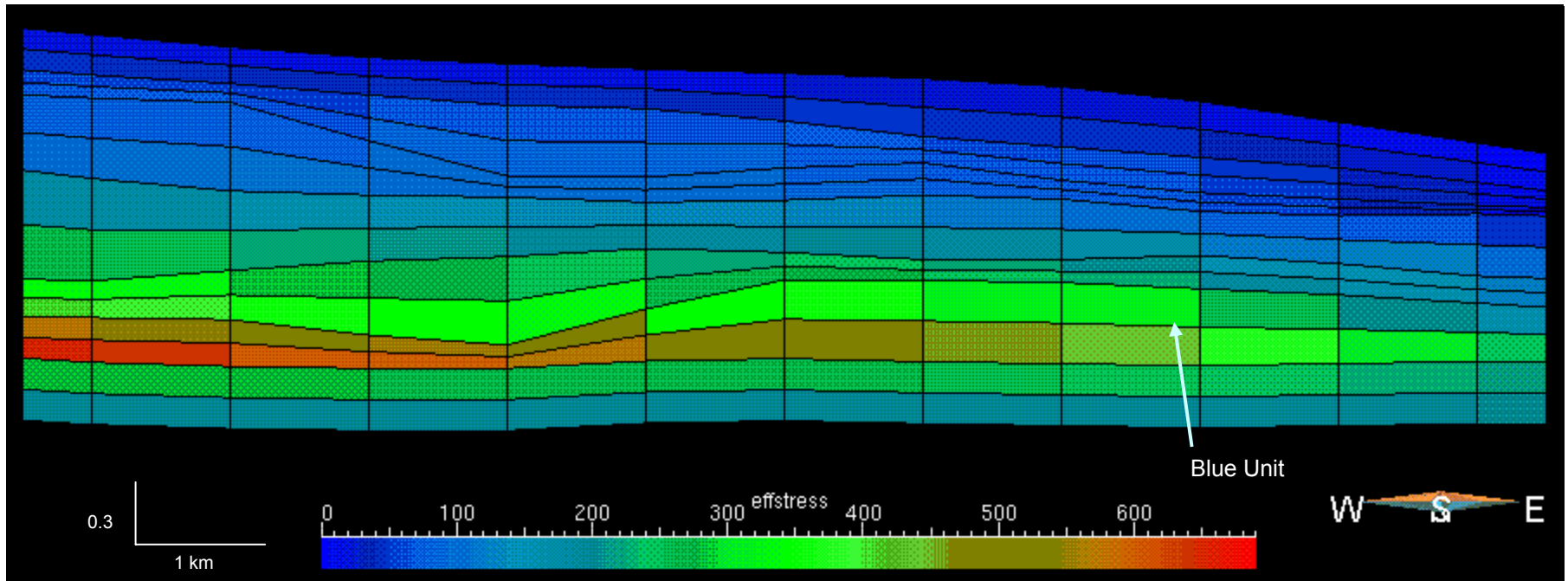
Figure 3-7: Effective stress (in psi) from the Stellar 2-D simulation is shown in cross-section after 80 ky of simulation. Effective stress is largest in the Blue Unit sand layer (third and fourth layers up from base) which sustains the least overpressures. Effective stress decreases to the right as the total sediment package thins. Model inputs are described in Section 3.4.

Figure 3-8
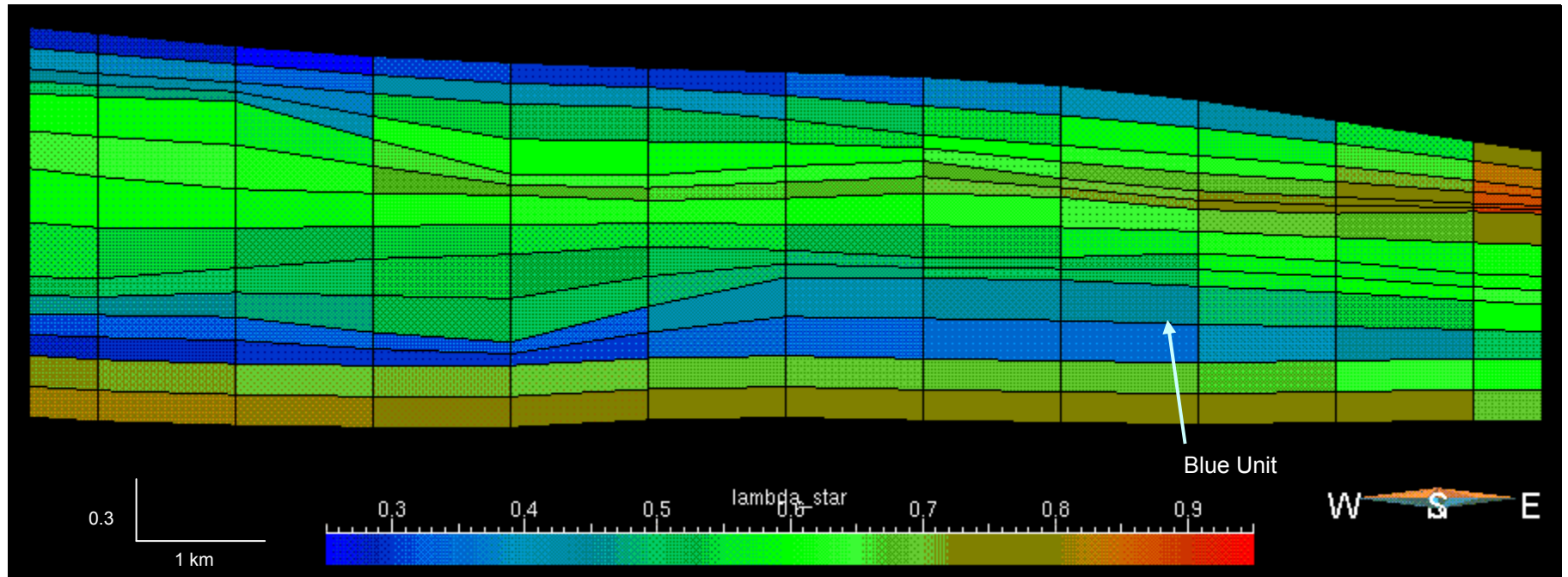
Figure 3-8: Overpressure ratio from the Stellar 2-D simulation is shown in cross-section after 80 ky of simulation. The location of the Blue Unit (third and fourth layers from the base) is highlighted. The highest overpressure ratio (90%) is observed in the toe of the wedge to the east of Site U1322. The base shale (bottom 2 layers below the Blue Unit) also shows an elevated overpressure ratio of 80%. Model inputs are described in Section 3.4.

Figure 3-9
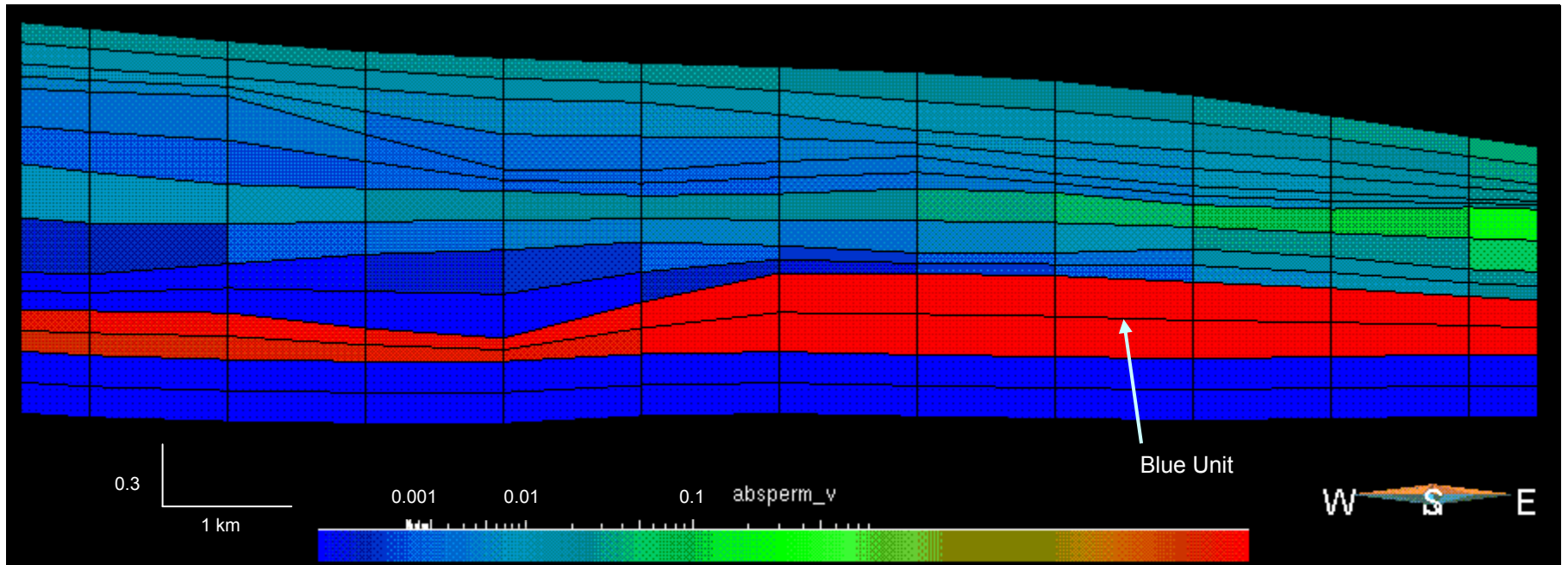
Figure 3-9: Permeability from the Stellar 2-D simulation is shown in cross-section after 80 ky of simulation. The highest permeability is observed in the Blue Unit (third and fourth layers from the base). Model inputs are described in Section 3.4.

Figure 3-10
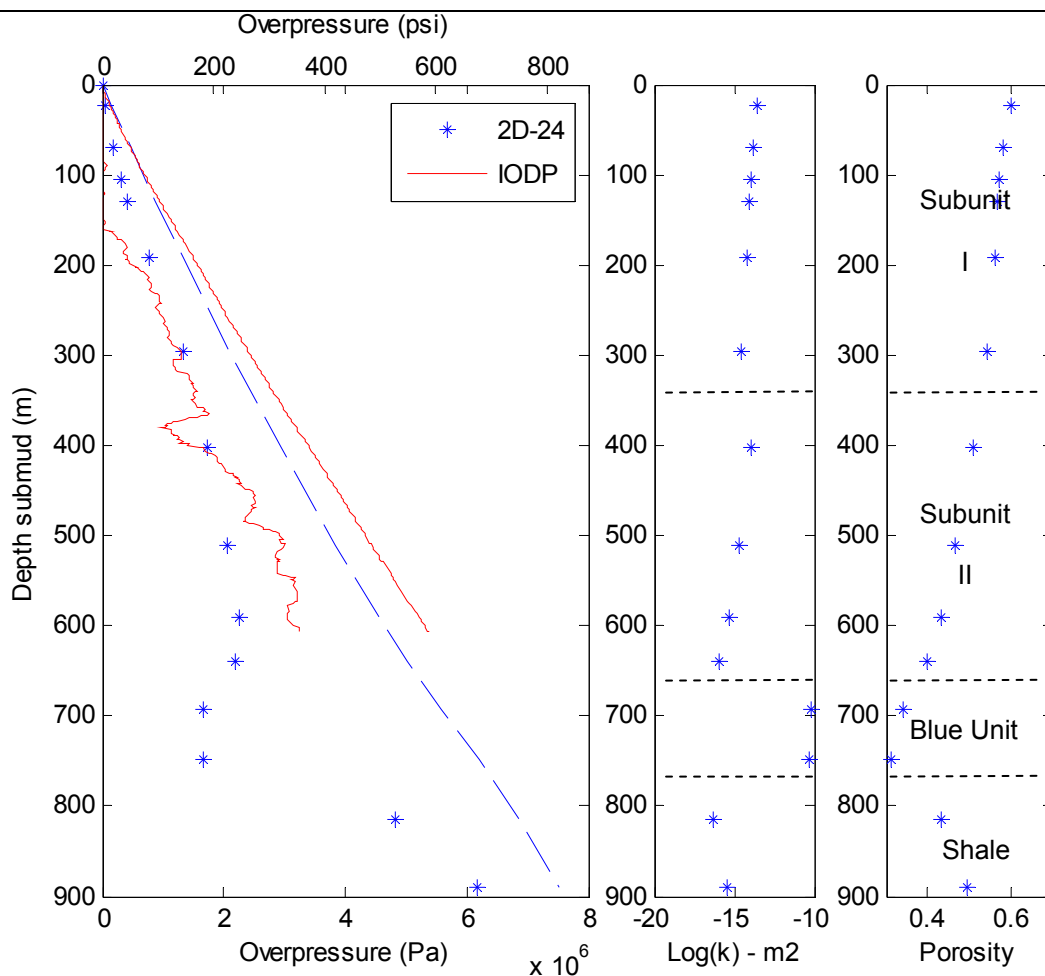
Figure 3-10: Overpressures from the Stellar™ 2-D simulation using permeability functions (2D-24 = blue dashed line) extracted at the simulated Site U1324 show more overpressure generation than the IODP estimates (IODP = red solid line). However, reduced overburden stress predictions (blue dashed line) agree closely. Permeability and porosity are shown at right. Model inputs are described in Section 3.4.

Figure 3-11
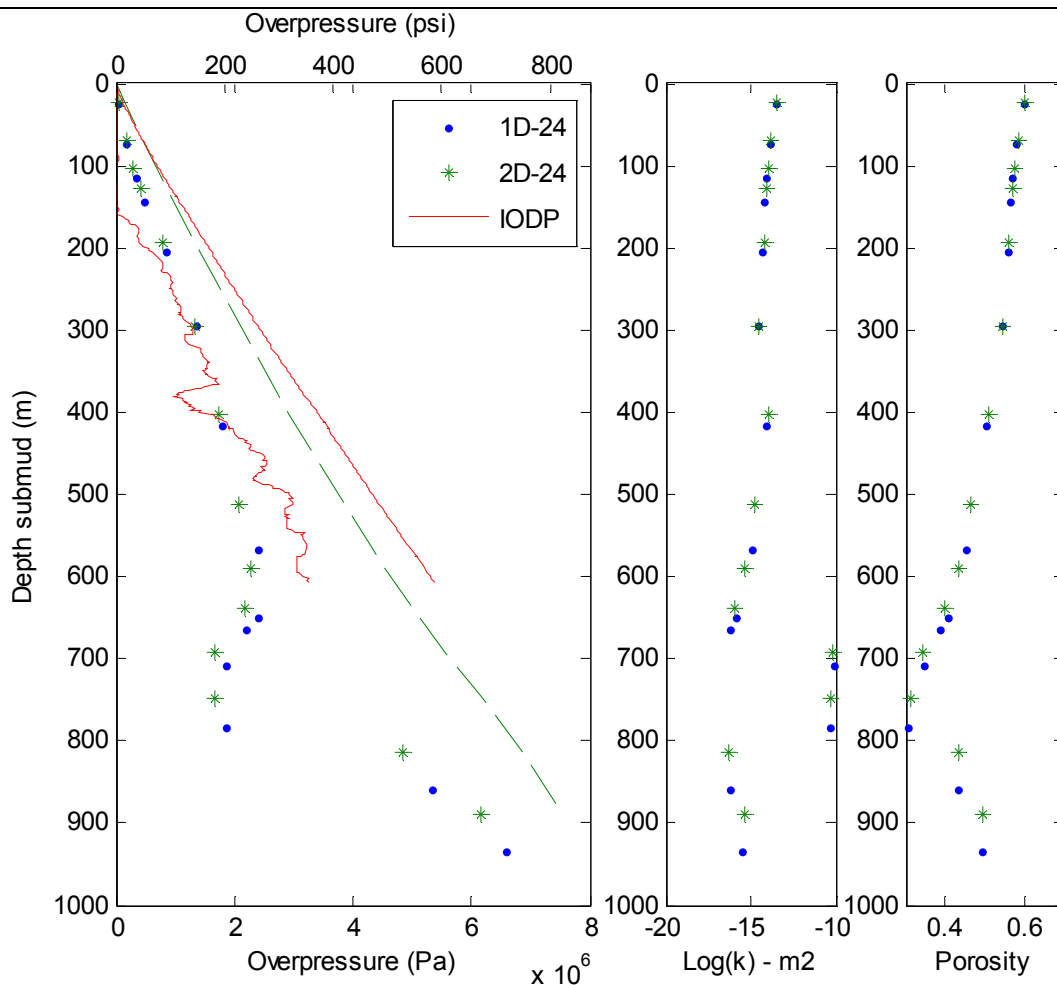
Figure 3-11: Results from Figure 3-3 are overlain with results from Figure 3-10. The 1-D simulation of Site U1324 (1D-24 = blue dots) predicts the same overpressure as does the 2-D simulation (2D-24 = green asterisks). Both models overpredict the IODP estimates (IODP = red solid line). Permeability and porosity are shown at right. Model inputs are described in Section 3.4.

Figure 3-12
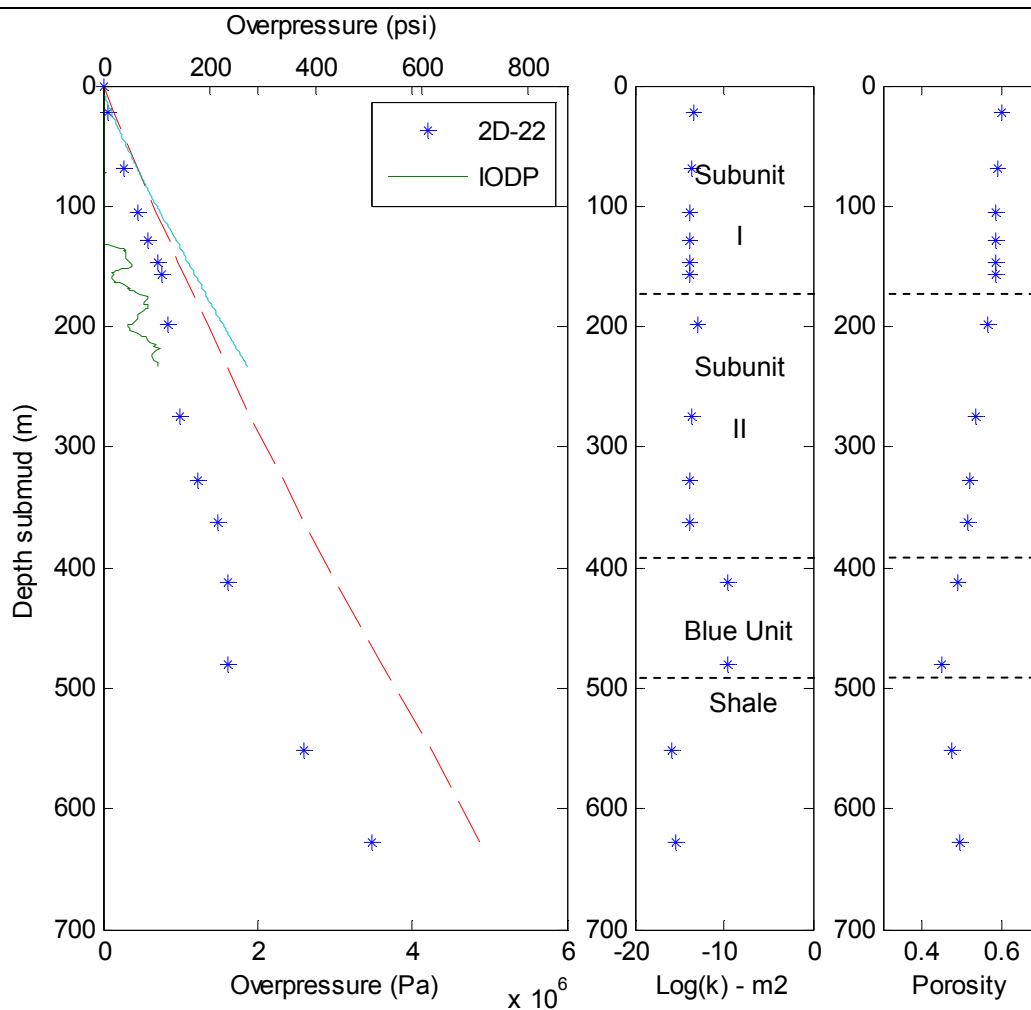
Figure 3-12: Stellar™ 2-D overpressures using permeability functions extracted slightly to the west of the simulated Site U1322 (2D-22 = blue asterisks) overpredict the IODP estimates (IODP = red solid line). Permeability and porosity are shown at right, with lithofacies labeled. Model inputs are described in Section 3.4.

Figure 3-13
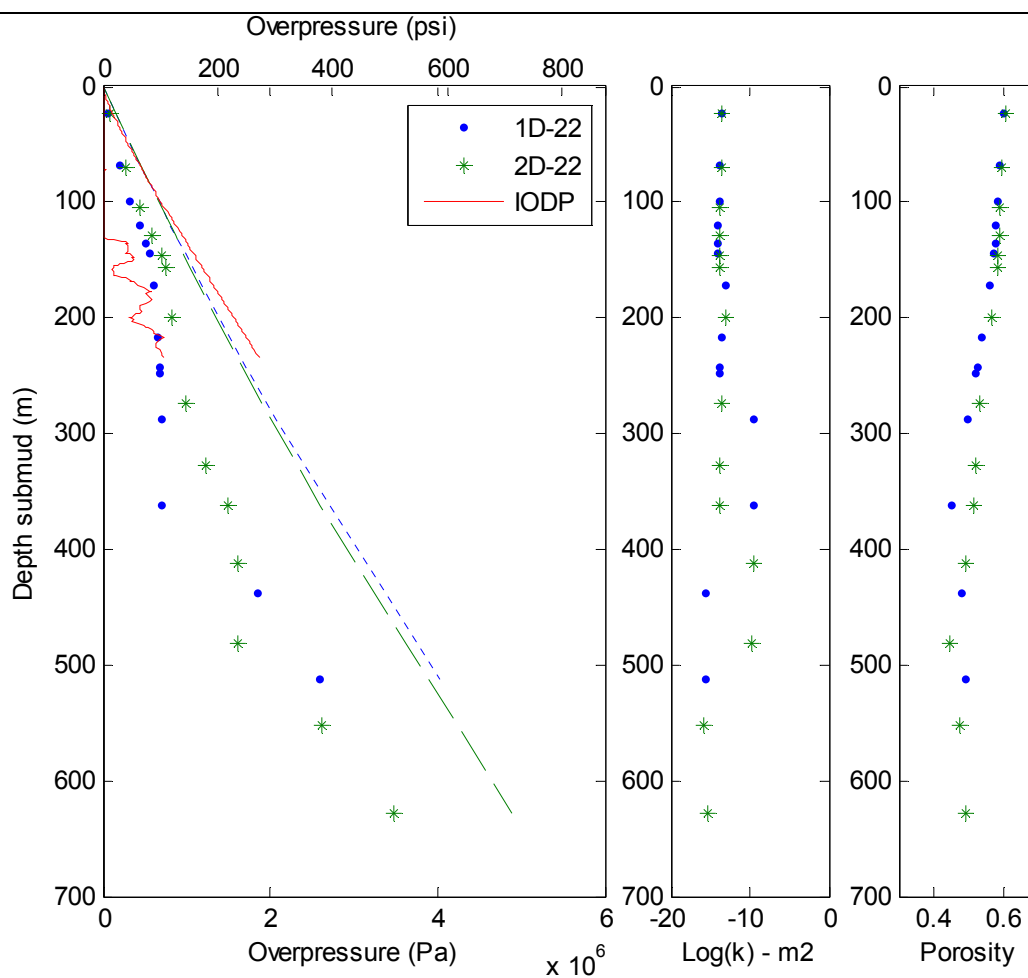
Figure 3-13: Results from Figure 3-4 are overlain with the results from Figure 3-12. The 2-D extraction of slightly to the west of Site U1322 (2D-22 - green asterisks) predicts higher overpressure than the 1-D simulation (1D-22 - blue dots). Both models overpredict the IODP estimates (IODP - red solid line). Permeability and porosity are shown at right with lithofacies labeled. Model inputs are described in Section 3.4.

Figure 3-14
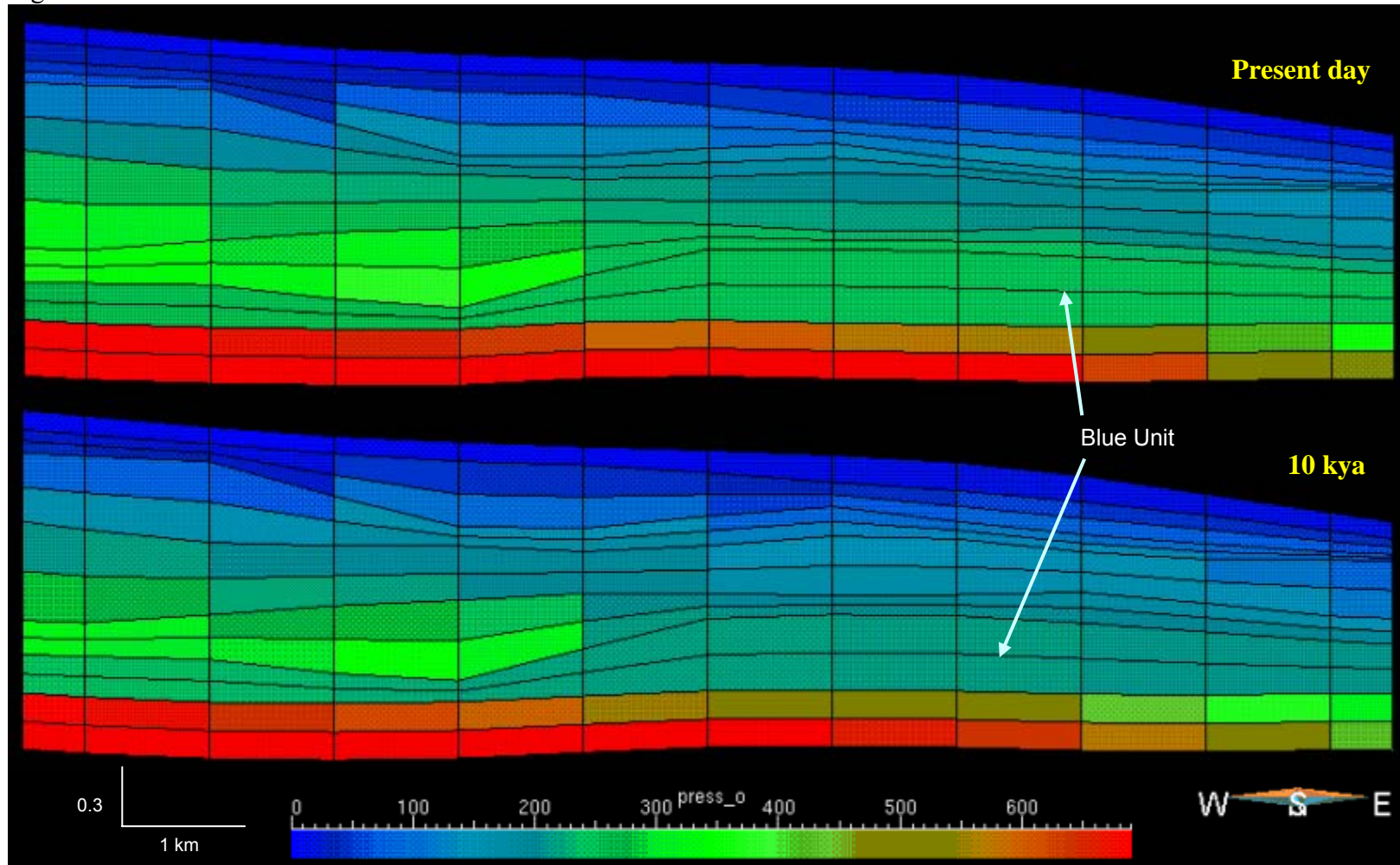
Figure 3-14: Results from the permeability function model show the development of overpressure (in psi) from 10 kya to present day. The location of the Blue Unit (third and fourth layers from the base in each cross-section) is highlighted.

Figure 3-15
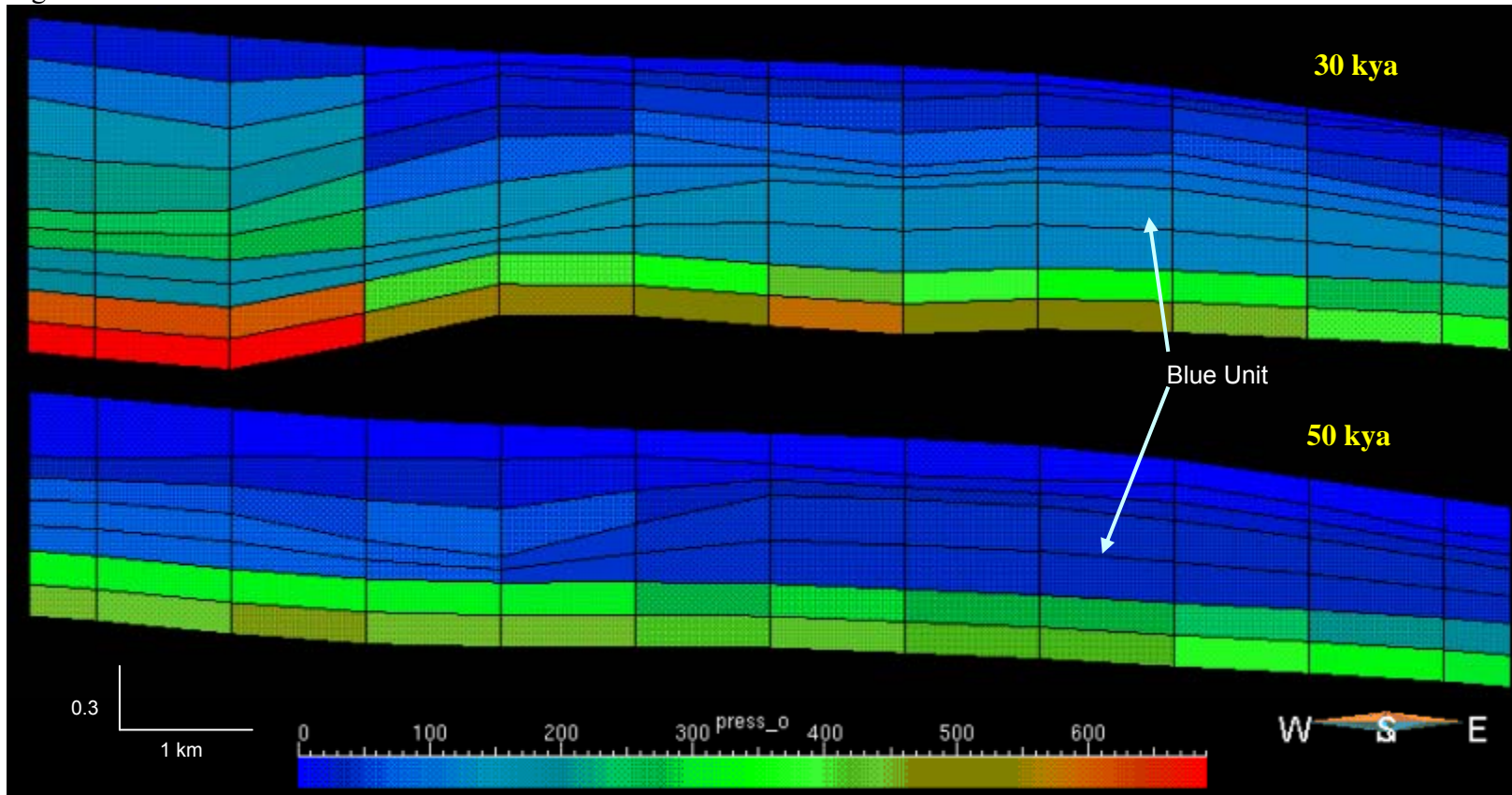
Figure 3-15: Results from the permeability function model show the development of overpressure (in psi) from 50 kya to 30 kya. Significant overpressure in the base shale (bottom two layers) is sustained from 30 kya. The location of the Blue Unit (third and fourth layers from the base in each cross-section) is highlighted. Model inputs are described in Section 3.4.

Figure 3-16
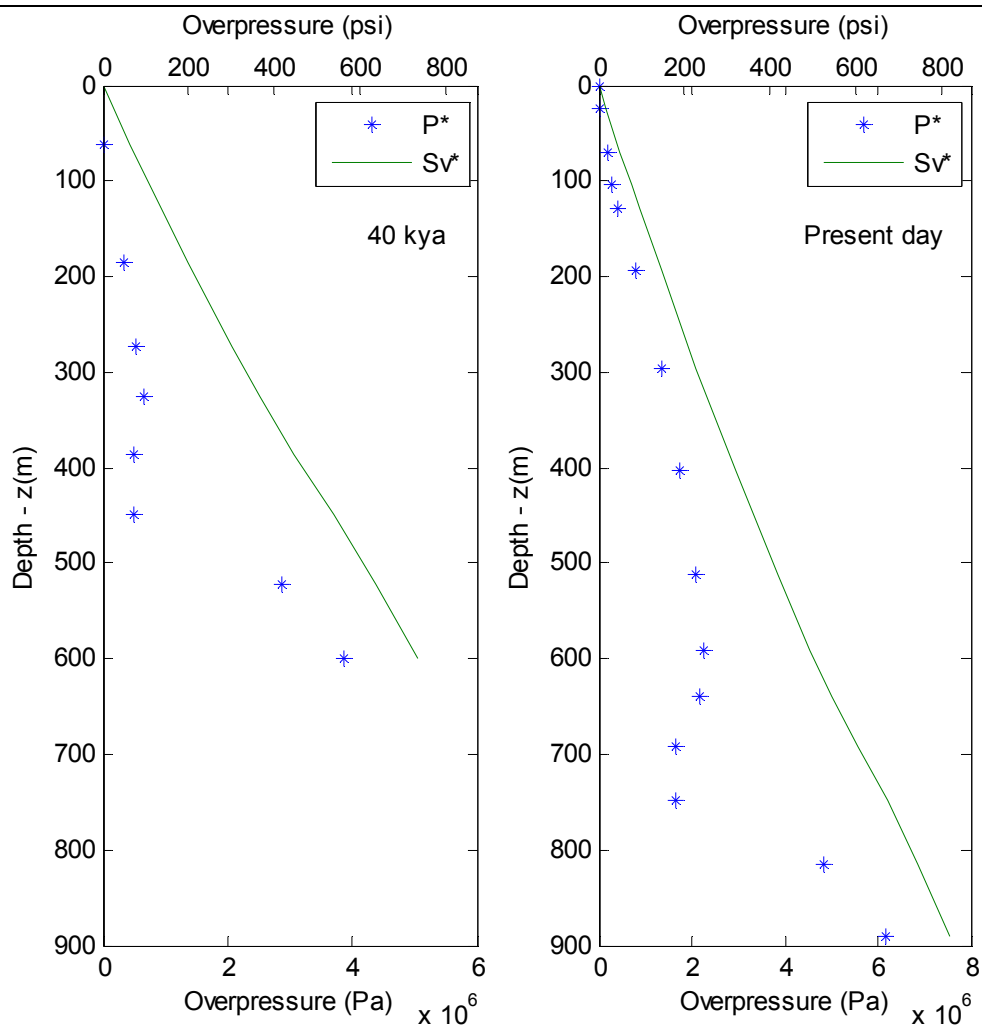
Figure 3-16: A 1-D extraction at Site U1324 from 40 kya (left graph) is compared to the present day (right graph). Overpressure (blue asterisks) is only sustained in the base shale which is at 600 mbsf compared to the present day depth of 900 mbsf. Reduced overburden stress (green line) is shown for reference.

3.5 Sensitivity Testing

To determine the uniqueness of the Ursa modeling results, additional testing using slight modifications of permeability was done. The magnitude of the initial permeability (k_0) was changed by 2-3 orders of magnitude from that used in the Ursa modeling simulation. The depositional history was not changed.

This test showed that the magnitude of the overpressure was strongly dependent on the permeability structure. For permeability 3 orders of magnitude higher than Ursa sediments ($k_0 \times 10^3$), no overpressure is maintained in the column and a hydrostatic result is observed, except in the basal shale layers. For permeability 2 orders of magnitude lower than Ursa ($k_0 \times 10^{-2}$), overpressure is elevated and is equivalent to the reduced overburden stress at the top of the sediment column (Figure 3-17).

To simulate the influence of a regional aquifer, constant pressure boundaries were imposed on the western face of the Blue Unit. Pressure was imposed as a fraction of the overburden stress and was maintained for the duration of the simulation once the Blue Unit was deposited (65 kya to present). Results are shown extracted from Site U1324 with 30 % and 60 % of the overburden stress imposed (Figure 3-18). When a 30 % pressure boundary was imposed, the overpressure result was identical to the Ursa simulation with no boundary condition imposed (Figure 3-10). With a 60 % pressure boundary imposed, overpressure was increased most significantly in the Blue Unit sands. The overpressure ratio in the sands increased from 30 % to nearly 50 %. There was little impact elsewhere in the sediment column.

These results are highlighted in the cross-section of overpressure in Figure 3-19. Due to the constant pressure gradient at the western end of the Blue Unit, there is an overpressure gradient within the Blue Unit sands. Overpresssure declines from west to east within the sands. This differs from the simulation in Section 3-4 where there was no boundary condition and the Blue Unit sands were at a constant overpressure (Figure 3-6). Effective stress is still largest within the Blue Unit (Figure 3-20). However, as the fluid pressure has increased in the sands, the effective stress decreased, relative to the result presented in Figure 3-7.

Figure 3-17
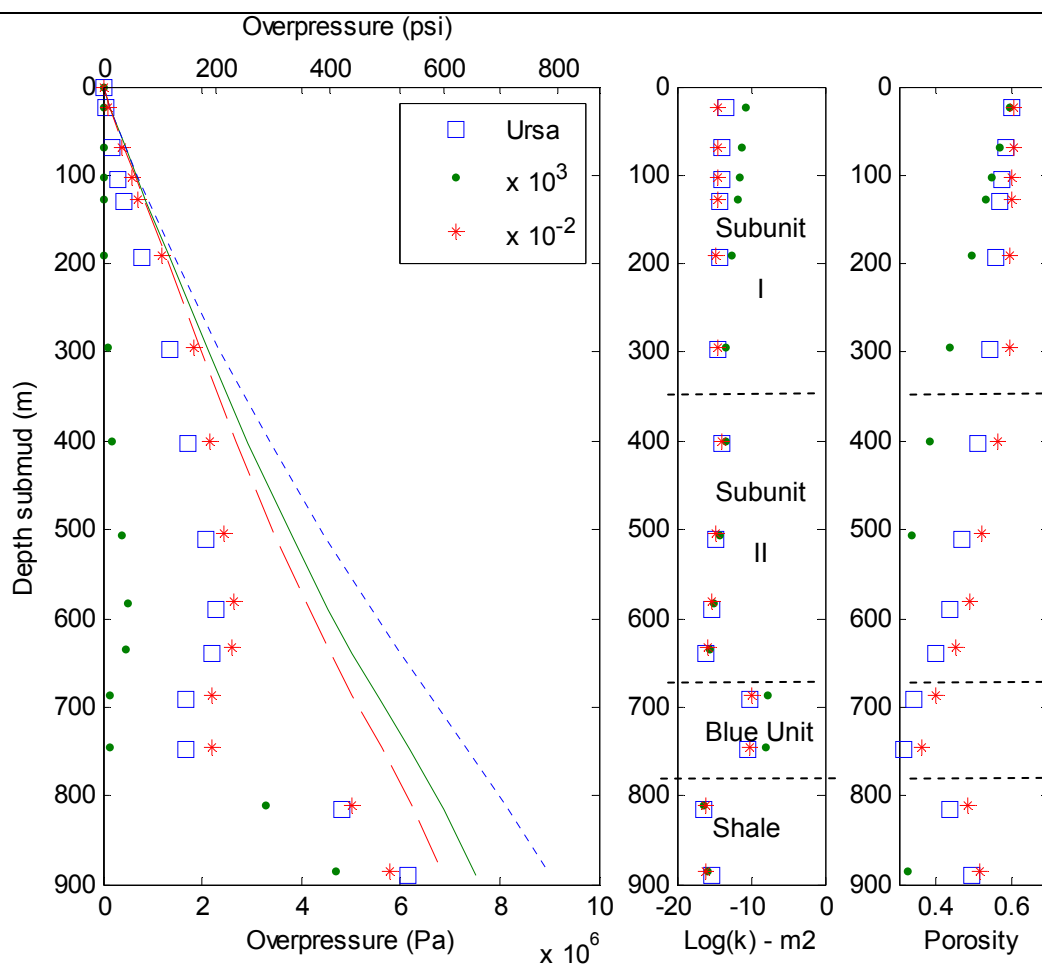
Figure 3-17: Overpressures are shown for model runs with initial permeability adjusted by 3 orders of magnitude higher (k x 10^3 = green dots) and 2 orders of magnitude lower (k x 10^{-2} = red asterisks). Results are compared with the Ursa Region model (Ursa = blue squares) of Figure 3-10. All results are extracted at simulated Site U1324. Permeability and porosity are shown on the right, with lithofacies labeled. Model inputs are described in Section 3.5.

Figure 3-18
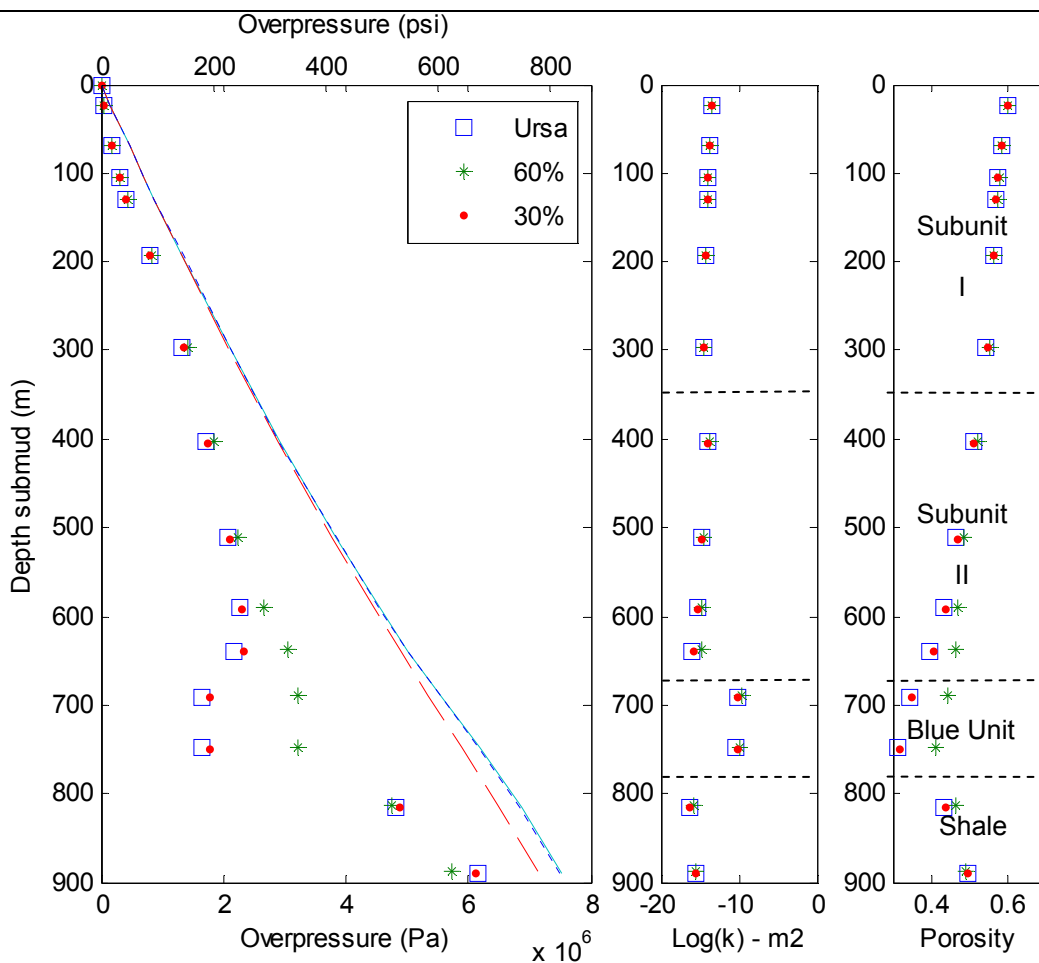
Figure 3-18: Overpressures are shown for model runs with constant pressure boundaries at 30 % (red dots) and 60% (green asterisks) of the overburden stress imposed on the western face of the Blue Unit. Results are compared with the Ursa Region model with closed boundary conditions (blue squares). Extractions are from simulated Site U1324. Permeability and porosity are shown on right with lithofacies labeled. Model inputs are described in Section 3.5.

Figure 3-19
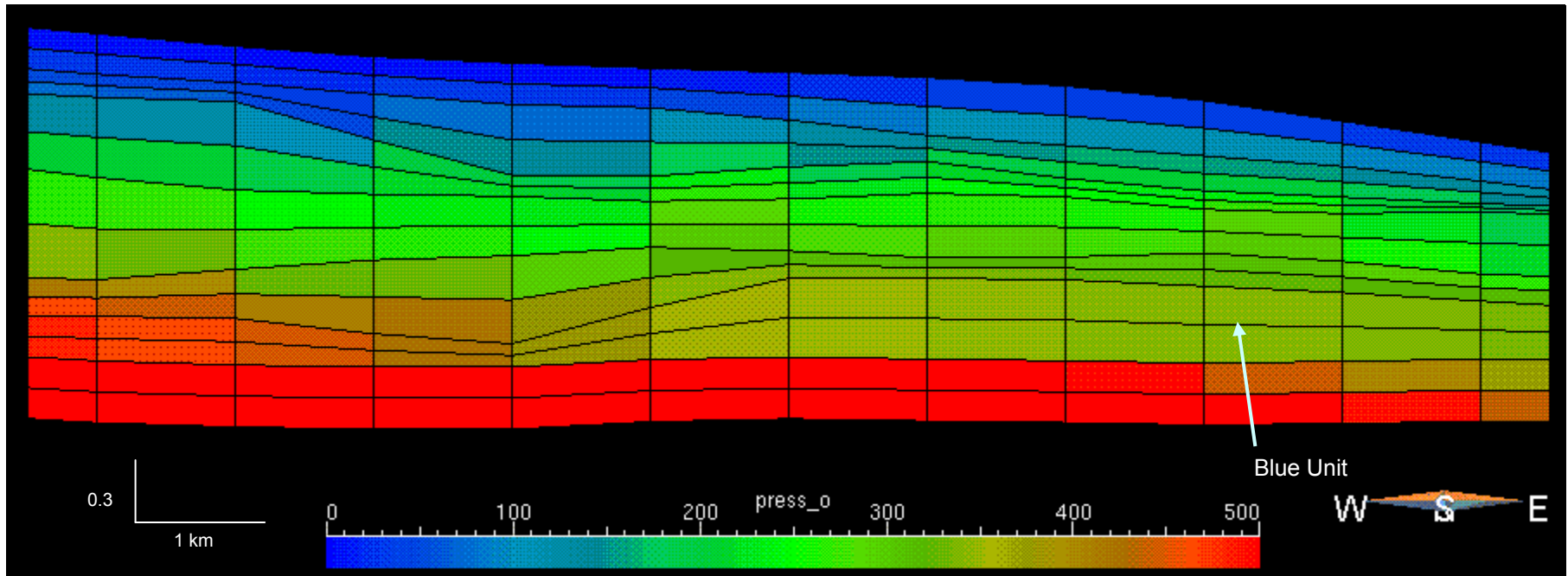
Figure 3-19: Overpressure (in psi) is shown in cross-section when a 60 % constant pressure boundary is imposed on the western face of the Blue Unit (third and fourth layers from the base). Compared to Figure 3-6, this boundary condition has caused a significant pressure gradient within the Blue Unit. Cell boundaries are shown in black. Model inputs are described in Section 3.5.

Figure 3-20
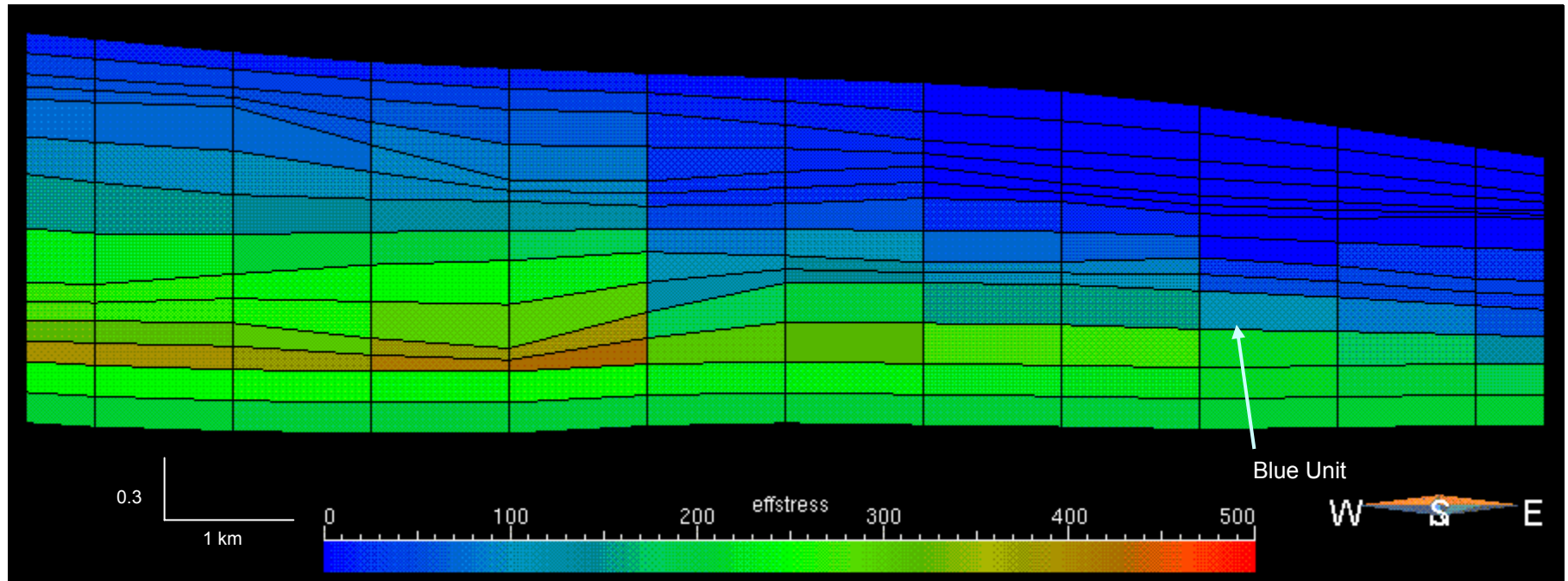
Figure 3-20: Effective stress (in psi) is shown in cross-section when a 60 % constant pressure boundary is imposed on the western face of the Blue Unit (third and fourth layers from the base). Compared to Figure 3-7, this boundary condition has caused a decline in the effective stress at the western end of the Blue Unit. Cell boundaries are shown in black. Model inputs are described in Section 3.5.

3.6 Discussion

Comparison of 1-D Stellar™ models with the Matlab® model of the previous chapter show very close agreement in the pressure signature of the simulations. The Stellar™ models slightly underpredict the numerical model, and show the closest agreement with low permeability simulations.

Results from the Ursa simulations performed with Stellar™ consistently overpredict the IODP overpressure estimates at shallow depths, but show good agreement within the sediment column. Simulation results do show a marked decrease in overpressure in the region from the west to the east. This pressure variation corresponds to an overall thinning of the sediment package. Additionally, comparison of 1-D and 2-D extractions indicates that there is increased overpressure at Site U1322, which may be an indication of lateral fluid flow towards this site. This result supports the hypothesis that the geometry of the sediments at Ursa result in focused flow towards the toe of the wedge.

Observation of the changes in overpressure with time show that significant overpressure is accumulated during the last 30 ky, during the deposition of the Subunit I lithofacies. This facies is of low permeability and was rapidly deposited, restricting fluid flow out of the Ursa Region.

Additional testing with variable permeabilities indicated that the overpressures are strongly dependent on the pressure functions used. For permeabilities higher than those

calculated for Ursa, little to no overpressure is developed. Permeabilities 100 times lower than the Ursa permeabilities result in overpressures that equal the reduced overburden stress at shallow depths. This latter result indicates that slope failure is likely to occur with rapid loading of such low permeability sediments.

Testing with boundary conditions to simulate an aquifer driving flow from the west showed very small overall impact on the overpressure of the overall sediment column. Only within the Blue Unit, where the pressure boundary was imposed, was there a significant increase in overpressure. This result suggests that the overpressure is retained within the sands and transferred laterally, rather than dissipating upwards through the sediment column. The overpressure gradient within the sands is additional evidence that fluid flow is likely to be significant within the sands. Thus a regional aquifer may explain why the overpressure is maintained within the sands, though it is not necessary to explain the overall overpressure of the Ursa Region.

In order to improve the model accuracy, the following may be considered:

(a) gridding and resolution – as with all numerical models, higher resolution or smaller grid cells produce more accurate results at the cost of computational efficiency. It may be useful to revisit the models with higher resolution to confirm that the low overpressures generated are not a result of numerical inaccuracy. The resolution of the model is limited by the resolution of the seismic data used to build the grids.

(b) statistical variation – the current model assumes homogenous lithology layers that are well connected laterally and vertically. A more realistic model may be constructed that includes statistical variation of the lithology, particularly in

terms of anisotropy. Additionally, a lithology map can be built to simulate random facies variation in the Ursa region. An improved model that relies on variation of seismic parameters may provide useful lithology maps.

3.7 Summary

Numerical models of sediment compaction illustrate that rapid sedimentation of low permeability sediments contribute to the high overpressure observed in the Ursa Region. Overpressure was generated during the last 30 kya, when deposition of the low permeability mud and clay comprising Subunit I occurred. The wedge geometry of the slope sediments caused a gradient in sedimentation rates across the region. Sedimentation rates at Site U1324 were 3 times much higher than those at Site U1322. Fluid pressures are elevated where the sedimentation rate was high and deposits are consequently thick. This gradient in fluid pressures continues to drive fluids towards the toe of the wedge.

Considering the shallow onset and the magnitude of overpressure at Ursa, a regional aquifer is a likely source to drive fluid into the sands and maintain the high overpressure signature. This theory was tested by implementing different boundary conditions to simulate an aquifer and found to add overpressure only in the Blue Unit layer. Additional compartments within the Blue Unit may also obstruct flow and allow pockets of overpressure to develop. Modeling with non-homogeneous layers can test the theory of compartmentalized overpressure.

Other non-mechanical pressure sources, such as thermal maturation and diagenesis, are not believed to produce the significant overpressures observed at Ursa, given the rapid sedimentation rates and compaction history. Nonetheless, they may contribute to overpressure at depth and help to maintain the near surface overpressure

observed in this study. Additional study to greater depths and including these additional sources may provide greater insight to the pressure and flow system at Ursa.

Bibliography

Audet, D. and Fowler, A. 1992. "A mathematical model for compaction in sedimentary basins." *Geophysics Journal International.* v110.p577-590.

Bethke, C. 1985. "A numerical model of compaction-driven groundwater flow and heat transfer and its application to the paleohydrology of intracratonic basins." *Journal of Geophysical Research*. v90. p6817-6828.

Bethke, C. 1986. "Inverse hydrologic analysis of the distribution and origin of Gulf Coast-type geopressured zones." *Journal of Geophysical Research*. v91. p6535-6545.

Bethke, C. and Corbet, T. 1988. "Linear and Nonlinear Solutions for One-Dimensional Compaction Flow in Sedimentary Basins". *Water Resources Research*. v24. p461-467.

Bredehoeft, J. and Hanshaw, B. 1968. "On the maintenance of anomalous fluid pressures, I, Thick sedimentary sequences". *Geological Society of America Bulletin*. v79. p1097-1106.

Chen, Z., Ewing, R., Lu, H., Lyons, S., Maliassov, S., Ray, M. and Sun, T. 2002. "Integrated two-dimensional modeling of fluid flow and compaction in a sedimentary basin" Computational Geosciences. v6. p545-564.

Dugan, B. and Flemings, P. 2000. "Overpressure and fluid flow in the New Jersey continental slope: implications for slope failure and cold seeps". *Science*, v289. p288-291.

Eaton, L. 1999. "Drilling through deepwater shallow water flow zones at Ursa". *Society of Petroleum Engineers/International Association of Drilling Contractors*. Amsterdam. p153-164.

Expedition 308 Scientists, 2005. "Overpressure and fluid flow processes in the deepwater Gulf of Mexico: slope stability, seeps, and shallow-water flow." *Integrated Ocean Drilling Program Preliminary Report, 308*. doi:10:2204/iodp.pr.308.2005

Flemings, P., Comisky, J., Liu, X. and Lupa, J. 2001. "Stress-controlled porosity in Overpressured Sands at Bullwinkle (GC65), Deepwater Gulf of Mexico." Proceedings of the Offshore Technology Conference, OTC Paper #13103.

Flemings, P., Stump, B., Finkbeiner, T. and Zoback, M. 2002. "Flow focusing in overpressured sandstones: theory, observations and applications". *American Journal of Science*, v302. p287-855

Fogg, G. 1986. "Groundwater flow and sand body interconnectedness in a thick multiple aquifer system". *Water Resources Research*, v22.p679-694

Fowler, A. and Yang, X. 1998. "Fast and slow compaction in sedimentary basins." *Journal of Applied Mathematics*.v59.p365-385.

Gibson, R. 1958. "The Progress of Consolidation in a Clay Layer Increasing in thickness with time." *Geotechnique*. v8. p171 – 182.

Gordon, D. and Flemings, P. 1998. "Generation of overpressure and compaction-driven flow in a Plio-Pleistocene growth-faulted basin, Eugene Island 330, offshore Louisiana." *Basin Research*, v10, p177-196.

Harrison, W. and Summa, L. 1991. "Paleohydrology of the Gulf of Mexico Basin." *American Journal of Science.* v291. p109-176.

Hart, B., Flemings, P. and Deshpande, A. 1995. "Porosity and pressure: role of compaction disequilibrium in the development of geopressures in a Gulf Coast Pleistocene basin." *Geology*. v23. p45-48.

Long, H. 2006. Personal communication.

Luo, X. and Vasseur, G. 1992. "Contribution of compaction and aquathermal pressuring to geopressure and the influence of environmental conditions." *American Association of Petroleum Geologists Bulletin*, v76. p1550-1559

Lupa, J. 2002. Geopressure and Flow Focusing on the slope of the Gulf of Mexico, GC65. Thesis. 98pp.

Palciauskas, V. and Domenico, P. 1989. "Fluid Pressures in Deforming Rocks." *Water Resources Research*. v25. p203-213.

Saywer, D., Flemings, P., Shipp, C. and Winker, C. in press. "Seismic Geomorphology, Lithology, and Evolution of the Late Pleistocene Mars-Ursa Turbidite Mini-Basin, Northern Gulf of Mexico". *American Association of Petroleum Geologists Bulletin.*

Turcotte, D. and Schubert, G. 2002. *Geodynamics*. Cambridge University Press.

Winker, C and Booth, J. 2000. "Sedimentary dynamics of the salt dominated continental slope, Gulf of Mexico; Integration of observations from the seafloor, near-surface, and deep subsurface". *SEPM Gulf Coast Section 20th Annual research Conference, December 3-6*. p1059-1086.

Winker, C and Shipp, R. 2002. "Sequence Stratigraphic Framework for Prediction of Shallow Water Flow in the Greater Mars-Ursa Area, Mississippi Canyon Area, Gulf of Mexico Continental Slope (abs.)" *SEPM Gulf Coast Section 22nd Annual Research Conference.*

Appendix A

Implementation of Model Equation and Finite-difference Approximation

Implementation of Model Equation

A conversion to compacted coordinates is used to simplify node tracking as element size changes due to compaction through time (Gordon and Flemings, 1998). This methodology also avoids calculation and tracking of large strains generated during compaction of sediments. In compacted coordinates, each element has the same number of grains and has no porosity. Spatial coordinates (dz) are mapped to the compacted coordinates ($d\eta$):

$$dz = \frac{1}{1-\phi}d\eta .$$

(A.1)

Porosity in the first element is initially assumed to be equivalent to the surface porosity. This value is projected to the midpoint of the element, and a corresponding element thickness, dz, value is determined. The porosity and spatial coordinates are tracked to determine the change in overburden stress due to this element, which is calculated using the bulk density equation:

$$\rho_b = \left(\phi\rho_f + (1-\phi)\rho_s\right).$$

(A.2)

The change in overburden, $d\sigma_v$, calculated from Equation A.3 is summed over the column to determine the total overburden, σ_v, at that depth.

$$d\sigma_v = \rho_b g dz .$$ (A.3)

The new value of σ_v is then used to determine porosity using the empirical porosity function defined by Hart et al. (1995):

$$\phi = \phi_0 e^{\beta(\sigma_v - P_f)} .$$ (A.4)

β is the matrix compressibility of the system, and P_f is the fluid pressure. Matrix compressibility is determined from consolidation experiments performed on cores from the Ursa Region and is assumed constant throughout the simulation. Fluid pressures are assumed hydrostatic at time of initial deposition.

By this iterative process, values of z, σ_v and φ are mapped from the compacted coordinates to spatial coordinates. Once a porosity profile is calculated, overpressure is calculated using the diffusion equation:

$$\frac{DP}{Dt} = \frac{K(1-\phi_\eta)^2}{S_t \rho g} \frac{D^2 P^*}{D\eta^2} .$$ (A.5)

In our numerical simulation, we assume that the rate of change of fluid pressure is equivalent to rate of change of overpressure. This holds true for any system where the fluid is approximately incompressible, as with water filled pores.

Finite-difference approximation

The numerical model is an implicit finite-difference solution of the diffustion equation with a central difference approximation in space:

$$\frac{dP_x}{dt} = \left[\frac{K_{x+1,x}(P_{x+1}^{t+1} - P_x^{t+1}) - K_{x,x-1}(P_x^{t+1} - P_{x-1}^{t+1})}{(dx)^2} \right]$$

$$where\ \ K_{x+1,x} = \frac{k_{x+1,x}}{\mu} \frac{(1-\phi_{x+1,x})^2}{St_{x+1,x}\rho_f g}. \tag{A.6}$$

Subscripts x, $x+1$ and $x-1$ refer to particular elements. As each element has a unique permeability (k), porosity (φ), and storage coefficient (St), average values must be calculated to evaluate flow between elements. From Darcy's law, the expression for flux is:

$$q = -K\frac{dP}{dx}. \tag{A.7}$$

Noting that at the interface, the flux for each element must be equivalent, and setting expressions for flux in each element equal, we obtain:

$$q = \frac{2}{dx} \frac{K_x K_{x+1}}{K_x + K_{x+1}} dP. \tag{A.8}$$

This result dictates that the harmonic mean of the values above and below the interface drives flow across that interface. The harmonic mean of the diffusivity for elements x and $x+1$ is calculated as:

$$K_{x,x+1} = \frac{(2K_x K_{x+1})}{dx(K_x + K_{x+q})}. \tag{A.9}$$

Solving the Finite-difference Equation

The initial condition and top boundary condition are fixed with zero overpressure. The base boundary condition is modelled as a no flow boundary. The finite-difference formulation for this basal condition is:

$$\frac{dP_x}{dt} = \left[\frac{K_{x-1,x}(P_{x-1}^{t+1} - P_x^{t+1})}{(dx)^2} \right]. \tag{A.10}$$

Expressed as a matrix for a 5-node system as an example, the solution matrix for a system with a constant pressure at the top and no-flow boundary at the base is written:

$$\begin{bmatrix} 1 & 0 & 0 & 0 & 0 \\ -K_{1,2} & 1+K_{1,2}+K_{2,3} & -K_{2,3} & 0 & 0 \\ 0 & -K_{2,3} & 1+K_{2,3}+K_{3,4} & -K_{3,4} & 0 \\ 0 & 0 & -K_{3,4} & 1+K_{3,4}+K_{4,5} & -K_{4,5} \\ 0 & 0 & 0 & -K_{4,5} & 1+K_{4,5} \end{bmatrix} \begin{Bmatrix} P_1^{t+1} \\ P_2^{t+1} \\ P_3^{t+1} \\ P_4^{t+1} \\ P_5^{t+1} \end{Bmatrix} = \begin{Bmatrix} P_1^t \\ P_2^t \\ P_3^t \\ P_4^t \\ P_5^t \end{Bmatrix}. \tag{A.11}$$

The matrix is solved by inversion.

Appendix B

1-D Consolidation Code

consolidateplus.m

```
%function consolidateplus(rhof, rhos, g, beta, b, dt, T, dn, n, N, eta0, phi0, m, H, bulk0, k)
% Louanne Christopher - consolidateplus.m
% Determine pressure and overpressure in compacted and spatial
% coordinate system using implicit finite-difference methods
% Calls compact.m, compact2.m, solve3.m as subroutines
%
% Base equation from Gordon and Flemings (1998)
% May 30, 2006

%clear all

% get code constants
[rhof, rhos, g, beta, b, dt, T, dn, n, N, eta0, phi0, m, H, bulk0, k] = values;


% uncomment lines below to run testing simulations
% testing analytical solution
%eta = linspace(0, 1200, 11); n = 11; N = n; dn = 120; m = 0; H = 0;
%[row, x] = full_analytical;
% testing Gibson solution
%[Pstar_gib, lambda_gib, lit_gib, x_gib, Pstar_dim, x_dim] = gibson_dim;

overP = zeros(T/dt,T/dt); press = zeros(T/dt,T/dt); lith = zeros(T/dt,T/dt);
pore = zeros(T/dt,T/dt); zdepth = zeros(T/dt,T/dt);

for t = 1:T
  t
  if t == 1
   % use initial eta field to generate initial z, phi, and pressure field
   % set initial overpressure field;
   Pstar(1:n) = 0;
   % generate porosity and sv table for time step 1
   [eta, dz, phi, sv] = compact(dn, n, phi0, eta0, beta, Pstar, rhos, rhof, g);
   init_porosity = phi; init_eta = eta;
   %phi(1:n) = phi0;
   % calculate bulk density
   bulk = (phi.*rhof + (1-phi).*rhos);
   % calculate sv
   [sv] = sumlith(dz, bulk, g, n);
   % calculate depth
   [depth] = sumdepth(dz, n);
```

```
% calculate coefficient for dsigma term
h = ((beta.*phi)./(1-phi)).*(1./(beta.*(phi./(1-phi))+(b.*phi)));
% calculate source term
source = h.*m*(bulk0)*g;
% add load and record new pressure values
P = rhof.*g.*depth + source;
Pstar = P - rhof.*g.*depth;
% establish boundary conditions
topbc = 0; botbc = (Pstar(1));

%elseif t == 2000
%    k(1) = 10^-13;
%   P = Pstar + rhof.*g.*depth;
    % load and calculate change in depth and effective stress
%[eta, dz, sig, phi, n, P, k] = compact2(dn, n, phi0, eta, beta, k, H, P, rhos, rhof, g);

% calculate bulk density
%bulk = (phi.*rhof + (1-phi).*rhos);
% calculate sv
%[sv] = sumlith(dz, bulk, g, n);
%[sv] = stress(sv,n, phi0, H, rhos, rhof, g);
% calculate depth
%[depth] = sumdepth(dz, n);
%[phi] = porecalc(n, phi0, beta, sv, P);

% calculate coeffiecient for dsigma term
%h = ((beta.*phi)./(1-phi)).*(1./(beta.*(phi./(1-phi))+(b.*phi)));
% recalculate source term
%source = h.*m*bulk0*g;
% add load and record new pressure values
%P = P + source; %Pstar +rhof.*g.*depth + source;
%Pstar = P - rhof.*g.*depth;
% establish boundary conditions in eta space
%topbc = 0; botbc = Pstar(1);

else
 P = Pstar + rhof.*g.*depth;

% load and calculate change in depth and effective stress
[eta, dz, sv, phi, n, P, k] = compact2(dn, n, phi0, eta, beta, k, H, P, rhos, rhof, g);
%phi = phi0;
%phi(1:n) = phi0;
% calculate bulk density
bulk = (phi.*rhof + (1-phi).*rhos);
% calculate sv
[sv] = sumlith(dz, bulk, g, n);
%[sv] = stress(sv,n, phi0, H, rhos, rhof, g);
% calculate depth
[depth] = sumdepth(dz, n);
%[phi] = porecalc(n, phi0, beta, sv, P);
%phi(1:n) = phi0;
% calculate coeffiecient for dsigma term
h = ((beta.*phi)./(1-phi)).*(1./(beta.*(phi./(1-phi))+(b.*phi)));
```

```
   % recalculate source term
   source = h.*m*(bulk0)*g;
   % add load and record new pressure values
   P = P + source; %Pstar +rhof.*g.*depth + source;
   Pstar = P - rhof.*g.*depth;
   % establish boundary conditions in eta space
   topbc = 0; botbc = Pstar(1);
   end

% reset initial overpressure field;
init = Pstar;

% use initial and boundary conditions to solve pressure diffusion equation
[Pstar] = solve3(dn, n, phi0, phi, k, beta, init, topbc, botbc, rhof, g);

% record new values at each dt time step
   if rem(t,dt) == 0
      overP((t/dt),1:n) = Pstar; press((t/dt),1:n) = Pstar + rhof.*g.*depth;
      lith((t/dt),1:n) = sv; pore((t/dt),1:n) = phi; zdepth((t/dt),1:n) = depth;
   end
end

C = numel(zdepth)/(T/dt);
lambda = Pstar./(sv-rhof.*g.*depth);

% record changes in effective stress and pressure
dp = []; dsv = [];
for count = 2:(T/dt)
   dpress = press(count,:)-press(count-1,:);
   dlith = lith(count,:)-lith(count-1,:);
   dp = [dp; dpress]; dsv = [dsv; dlith];
end

P = Pstar + rhof.*g.*depth;

% load and calculate change in depth and effective stress
%[eta, dz, sv, phi, n, P, k] = compact2(dn, n, phi0, eta, beta, k, H, P, rhos, rhof, g);
%phi(1:n) = phi0;
% calculate bulk density
%bulk = (phi.*rhof + (1-phi).*rhos);
% calculate sv
%[sv] = sumlith(dz, bulk, g, n);
%[sv] = stress(sv,n, phi0, H, rhos, rhof, g);
% calculate depth
%[depth] = sumdepth(dz, n);
%[phi] = porecalc(n, phi0, beta, sv, P);

svstar = sv-(rhof.*g.*depth);
tf = ((m^2)*t)./((k.*60.*60.*24.*365.25)./(rhof.*g.*(beta.*phi*10^-3)./(1-phi)));
dimlesP = Pstar./(h*(bulk0-rhof)*g*depth(1));
dimlesZ = depth./depth(1);

%save simresults.mat
```

compact.m

```
function [eta, depth, phi, sv] = compact(dn, n, phi0, eta0, beta, Pstar, rhos, rhof, g)
% Algorithm to determine initial porosity field, spatial coords
% and overburden based on initial compacted coordinate system
% March 24, 2006

porosity =[]; sv = []; depth= []; dz(1:n) = 0; sig(1:n) = 0;

for count = 1:n
   % eta = compacted coords referenced at center of each node
   eta(count) = eta0 + dn*(count-1);
   end
eta = fliplr(eta);

% calculate spatial coordinates and change in effective stress
% for top element
dz(n) = 2*(1/(1-phi0))*0.5*(eta(n) - 0); depth(n) = dz(n);
sig(n) = (phi0*rhof + (1-phi0)*rhos)*g*(dz(n)); sv(n) = sig(n);
phi(n) = phi0.*exp(-beta.*(sig(n) - rhof*g*dz(n)));

for nnodes = 1:n-1

   % calculate spatial coordinates and change in effective stress
   % for all other elements
   dz(n-nnodes) = (1/(1-phi(n-nnodes+1)))*(eta(n-nnodes) - eta(n-nnodes+1));
   sig(n-nnodes) = (phi(n-nnodes+1)*rhof + (1-phi(n-nnodes+1))*rhos)*g*dz(n-nnodes);

depth(n-nnodes) = sum(dz(n-nnodes:n));  % depth = true reference coords
sv(n-nnodes)= sum(sig(n-nnodes:n));     % total lithostatic stress at every depth
phi(n-nnodes) = phi0.*exp(-beta.*(sv(n-nnodes) - rhof*g*depth(n-nnodes)));
end
```

compact2.m

```
function [eta, dz, sv, phi, n, P, k] = compact2(dn, n, phi0, eta, beta, k, H, P, rhos, rhof, g)
% Function to convert spatial coords from compacted coords
% based on porosity.
% March 24, 2006

sv = []; dz(1:n) = 0; sig(1:n) = 0;

% add additional nodes if element has grown larger than node size
% nodes are numbered from the top down
if eta(n) > dn/2
   eta(n+1) = (eta(n) - 0.5*dn)*0.5;
   eta(n) = eta(n+1)/2 + 0.5*dn;
   dz(n+1) = (1/(1-phi0))*(eta(n+1)-0); depth(n+1) = dz(n+1);
for count = 1:n-1
   eta(n-count) = eta(n-count+1) + dn;
end
% renumber permeability values
   k(n+1) = k(n);
% update number of nodes
   n = n+1; P = [P rhof*g*dz(n)];
else
end


eta(n) = eta(n)+ H/2;
dz(n) = (1/(1-phi0))*(eta(n)-0);
% calculate change in effective stress at top node
sig(n) = (phi0*rhof + (1-phi0*rhos))*g*(dz(n)); sv(n) = sig(n);
phi(n) = phi0.*exp(-beta.*(sig(n) - P(n))); depth(n) = dz(n);

for nnodes = 1:n-1

eta(n-nnodes) = eta(n-nnodes)+ H;
dz(n-nnodes) = (1/(1-phi(n-nnodes+1)))*(eta(n-nnodes) - eta(n-nnodes+1));
% calculate change in effective stress at all other nodes
sig(n-nnodes) = (phi(n-nnodes+1)*rhof + (1-phi(n-nnodes+1))*rhos)*g*dz(n-nnodes);

depth(n-nnodes) = sum(dz(n-nnodes:n));
% calculate total effective stress
sv(n-nnodes) = sum(sig(n-nnodes:n));
% calculate porosity at node
phi(n-nnodes) = phi0*exp(-beta.*(sv(n-nnodes) - P(n-nnodes)));
end
```

solve3.m

```
function [Pstar] = solve3(dn, n, phi0, phi, k, beta, init, topbc, botbc, rhof,g)
% Implicit finite-difference solution of 1-D mass diffusion equation
% with spatially varying storage and permeability conditions.
% Used as subroutine in consolidateplus.m and consolidateplus_ursa.m
% March 30, 2006


N = n;
Z = (n)*dn;
x = linspace(0,Z,N);
dx = mean(diff(x));
dt = 1; yr =(60*60*24*365.25);

Fo = dt/(dx^2);
k = fliplr(k);
phi = fliplr(phi);
kp = (1.682*10^-13).*exp(phi./(0.125.*(1-phi)));
mu = 1; 10^-3;

% set constants: a - solid compressibility, b - fluid compressibility
% B = permeability / viscosity (Pa s)
B = yr.*(kp./mu).*(1/(rhof*g));

b = 0; %5^-10;

% calculate storage coefficient
St = B.*((1-phi).^2)./(beta.*(phi./(1-phi))+(b.*phi));

for s = 1:N-1
   % calculate the harmonic mean of the storage coefficient
   Sth(s)= 2*(St(s+1)*St(s))/(St(s+1)+St(s));
end
%Sth = St;

ma = zeros(N,N);
% set matrix terms for upper boundary
ma(1,1) = 1;

% set matrix terms for inner nodes
for count = 2:N-1
   % calculate lower diagonal terms
   ma(count, count-1) = -Fo*Sth(count-1);
   % calculate diagonal terms
   ma(count, count) = 1 + Fo*Sth(count-1) + Fo*Sth(count);
   % calculate upper diagonal terms
   ma(count, count+1) = -Fo*Sth(count);
end
```

```
% calculate matrix terms for bottom boundary
ma(N,N-1) = -Fo*Sth(N-1); ma(N,N) = 1+Fo*Sth(N-1);

% set initial condition for pressure field
Pstar = [fliplr(init)];
% boundary conditions
Pstar(1) = topbc; %Pstar(N) = botbc;

if N > numel(init)
    Pstar = [topbc init]; %Pstar(N) = botbc;
end

    overP(1:N) = ma\Pstar(1:N)';
    Pstar = fliplr(overP);
```